

Citation for published version:

Shen, J, Jeyhanipour, A, Richards, BS & Schäfer, AI 2019, 'Renewable energy powered membrane technology: Experimental investigation of system performance with variable module size and fluctuating energy', *Separation and Purification Technology*, vol. 221, pp. 64-73. <https://doi.org/10.1016/j.seppur.2019.03.004>

DOI:

[10.1016/j.seppur.2019.03.004](https://doi.org/10.1016/j.seppur.2019.03.004)

Publication date:

2019

Document Version

Peer reviewed version

[Link to publication](#)

Publisher Rights

CC BY-NC-ND

University of Bath

General rights

Copyright and moral rights for the publications made accessible in the public portal are retained by the authors and/or other copyright owners and it is a condition of accessing publications that users recognise and abide by the legal requirements associated with these rights.

Take down policy

If you believe that this document breaches copyright please contact us providing details, and we will remove access to the work immediately and investigate your claim.

1 **Renewable energy powered membrane technology:**
2 **experimental investigation of system performance with**
3 **variable module size and fluctuating energy**

4
5 *Junjie Shen^{1,2,3}, Azam Jeihanipour⁴, Bryce S. Richards^{2,4}, Andrea I. Schäfer^{3,5*}*

6
7 ¹ *Centre for Advanced Separations Engineering, University of Bath, Bath BA2 7AY,*
8 *United Kingdom*

9 ² *School of Engineering and Physical Sciences, Heriot-Watt University, Edinburgh*
10 *EH14 4AS, United Kingdom*

11 ³ *Water and Environmental Science and Engineering, Nelson Mandela African Institute of Science*
12 *and Technology, Arusha, Tanzania*

13 ⁴ *Institute of Microstructure Technology (IMT), KIT, Hermann-von-Helmholtz-Platz 1, 76344*
14 *Eggenstein-Leopoldshafen, Germany*

15 ⁵ *Membrane Technology Department, Institute of Functional Interfaces (IFG-MT), Karlsruhe*
16 *Institute of Technology, Hermann-von-Helmholtz-Platz 1,*
17 *76344 Eggenstein-Leopoldshafen, Germany*

18
19
20 **Separation and Purification Technology**

21
22 Submitted **9 April 2018**

23 Resubmitted **12 November 2018 & 2 March 2019**

24
25
26
27
28
29
30
31
32 *corresponding author: Prof. Andrea I. Schäfer, +49 (0)721 608 26906,
33 Andrea.Iris.Schaefer@kit.edu

34 **Abstract**

35 Integration of renewable energy and membrane filtration technologies such as nanofiltration
36 (NF) and reverse osmosis (RO) can provide drinking water in places where freshwater is scarce and
37 grid electrical connections are unavailable. This study investigated a directly-connected photovoltaic-
38 powered membrane system under fluctuating solar conditions. Specifically, two configurations of
39 NF/RO membranes with the same membrane area were investigated: a) 1× 4" module, which
40 contained one 4" NF/RO element; and b) 3× 2.5" module, which contained three 2.5" NF/RO
41 elements in series. A high fluoride brackish water ($[F^-] = 56.2$ mg/L, total dissolved solids [TDS] =
42 4076 mg/L) collected from northern Tanzania was treated by different membranes in the two
43 configurations. Performance indicators such as flux, specific energy consumption, and permeate F^-
44 concentration were monitored over a 60-min period of energy fluctuation that are part of a typical
45 solar day. The results showed that the overall performance of the 1× 4" module was superior to that
46 of the 3× 2.5" module. This is because the performance of a 3× 2.5" module degraded significantly
47 from the first element to the third element due to the increased feed concentration and the decreased
48 net driving pressure. Three 1×4" modules (BW30, BW30LE and NF90) and one 3×2.5" module
49 (BW30) were able to meet the drinking water guideline for fluoride. During cloud periods, the
50 transient permeate F^- concentration exceeded the guideline value due to insufficient power, however
51 the cumulative permeate F^- concentration was always well below the guideline. The photovoltaic-
52 powered membrane system equipped with the above modules provides a promising solution for
53 addressing drinking water problems in remote and rural areas.

54

55

56 **Keywords:** brackish water; desalination; module size; fluoride; energy fluctuation; nanofiltration;
57 reverse osmosis

58

59

60

61 **1. Introduction**

62 The ever-increasing demand for fresh water and clean energy are among the major issues that
63 humans will face and need to solve in the 21st century [1]. The two issues are intertwined via the
64 energy-water nexus, meaning here that drinking water treatment and supply will always require
65 energy [2]. Extreme cases can be found in the many remote locations in both developed and
66 developing countries, which are far away from both centralized water and grid electricity supplies,
67 and where natural freshwater resources are scarce as well [3, 4]. In such cases, the integration of
68 renewable energy (RE) technologies with membrane filtration technologies, namely nanofiltration
69 (NF) and reverse osmosis (RO), provides a sustainable solution for this issue [3-5]. For example,
70 many photovoltaic (PV) powered membrane systems have been successfully implemented throughout
71 the world [6-10]. The figure-of-merit for system performance is typically the specific energy
72 consumption (SEC, units: kWh/m³), which represents how much electricity is required to produce
73 1 m³ of clean drinking water. The SEC is dependent on feed water salinity, system size, and
74 membrane type [3, 11].

75 In most PV-powered membrane systems, batteries are used to compensate for variations in
76 solar irradiance [6, 8, 12, 13]. Nevertheless, batteries exhibit several disadvantages such as reducing
77 the overall system efficiency, high capital and maintenance costs, and potential negative
78 environmental impacts in case of improper disposal [7, 14]. Therefore, it has been suggested to avoid
79 the use of batteries in such membrane systems to increase the efficiency and robustness, while
80 decreasing costs [9, 14-16]. However, in such batteryless systems the DC power produced by the PV
81 modules is directly coupled to the pump motor. The system is naturally subjected to widely varying
82 energy availability, which arises from the Earth's rotation, as well as landscape and weather
83 conditions, such as clouds, wind and ambient temperature [17]. The fluctuating current produced by
84 the PV modules subjects the NF/RO membranes integrated into such systems to fluctuations in
85 pressure and flow rate, which affects their flux and permeate water quality [9, 14, 18]. Additionally,
86 manufacturer of NF/RO membranes typically recommend to operate the membrane system in a
87 constant permeate flow rate to increase the life time of the membrane [19]. Richards *et al.* [18]
88 investigated the effects of fluctuating energy on retention of dissolved contaminants from real water
89 using a PV-powered NF/RO system. It was found that fluctuations in pressure and feed flow, as a
90 result of variation in solar irradiance, impacted the removal of solutes whose retention mechanism
91 was convection/diffusion. However, solutes that were retained via size exclusion and charge repulsion
92 were not affected by fluctuations in solar energy. It has been shown that when a batteryless PV-
93 powered NF/RO system was working under fluctuating conditions, even though the flux was often
94 low, a satisfactory quality of water at a low SEC could be delivered [17, 20]. Further, there is a

95 potential for the NF/RO membrane to possibly benefit from steps in the solar irradiance due to
96 disruption of the concentration polarization layer via a naturally induced backwash occurring when
97 the pump switched off [17].

98 Currently, spiral wound (SW) modules are the most widely used membrane modules for
99 NF/RO, thanks to their large membrane packing area, high design flexibility, and manufacturability
100 [21]. The construction of a typical SW module can be found in Figure S1. The basic component in a
101 SW module is membrane envelope, which is made of two flat-sheet membranes sealed on three edges,
102 with a permeate carrier filled in between [22, 23]. The achievable performance of a SW module
103 depends not only on the physicochemical characteristics of membrane active surface, but also on the
104 module size parameters, such as membrane envelope number and membrane dimensions [22, 24].
105 However, there has been little research conducted on the effect of module size on batteryless PV-
106 powered membrane systems. Knowledge of the performance of different module sizes under energy-
107 fluctuating conditions is needed for system planning and design, especially for remote and developing
108 areas. It should be noted that during operation with fluctuating energy feed flow and transmembrane
109 pressure vary. This means that pressure drop, concentration polarization (and with this the osmotic
110 pressure at the membrane surface) vary significantly more than in conventionally operated membrane
111 systems. Further, the availability of direct current (DC) equipment such as pumps that are suitable
112 for small systems remains limited. In a scenario where salinity is high, rejection is high and
113 permeability is good and the pressure that can be supplied by the pump is limited, the osmotic pressure
114 may exceed the applied pressure and water permeation is no longer possible. This is typically most
115 likely to happen at the outlet of the module, while during fluctuation this scenario may be more
116 common. In consequence, the design cannot always maintained ideal and studies are aimed at finding
117 the safe operating window (SOW) for a particular water. Remaining within this SOW is a matter of
118 a suitable control system.

119 This paper addresses this knowledge gap by utilizing two types of SW modules (with
120 comparable membrane areas) in treating a Tanzanian brackish water with high fluoride contents. In
121 Tanzania, excessive fluoride in drinking water has been recognized to cause large-scale health
122 problems, including dental and skeletal fluorosis [25-27]. Current defluoridation methods available
123 in Tanzania, such as adsorption and precipitation, are far from satisfactory due to insufficient removal
124 capacity and complicated maintenance [28-30]. Previous work from has demonstrated that NF/RO
125 membranes are effective in removing fluoride from natural waters in Tanzania [10, 20, 31]. In this
126 study, a batteryless PV-powered membrane system with two types of SW modules will be operated
127 under energy fluctuations. Variations of operating parameters (pressure, feed flow) and performance
128 indicators (flux, SEC, permeate concentration) of the two modules will be compared. In addition, the

129 performance degradation of each element within the 3× 2.5" module will be investigated. The
130 concentration polarization of such operation was calculated for three energy levels observed from the
131 experimental study using computational fluid dynamics (CFD) for this variable module configuration
132 to understand the transport phenomena [32].
133

134 2. Materials and methods

135 2.1. Water characteristics

136 A high fluoride content brackish water from a borehole in Mdori, a remote village near Lake
137 Manyara in northern Tanzania (GPS coordinates: S03°47.273', E035°51.138'), was used as natural
138 water to be treated by NF/RO. 5000 L of water was collected by a water truck on 17 January, 2014.
139 The pH and electrical conductivity (EC) were measured by a pH/conductivity meter (Multi 340i,
140 WTW, Germany). Turbidity was measured using a turbidity meter (TN100, Eutech, Netherlands).
141 Total organic carbon (TOC) and inorganic carbon (IC) were determined by a portable TOC analyzer
142 with autosampler (Sievers 900, GE Analytical Instruments, USA). Fluoride ion (F⁻) was determined
143 by an ion-selective electrode connected to a pH meter (826 pH Mobile Meter, Metrohm, UK).
144 Chloride (Cl⁻) and sulphate (SO₄²⁻) ions were analyzed by an ion chromatograph (IC 790, Metrohm,
145 Germany). Metal and non-metallic elements were measured via inductively coupled plasma optical
146 emission spectrometry (ICP-OES) (Vista-PRO CCD Simultaneous ICP-OES, Varian, Netherlands).
147 Methods of IC and ICP-OES were described by Shen et al. [20]. Total dissolved solid (TDS) was
148 calculated as the sum of major cations and anions.

149 The water quality components are presented in Table 1. The water was characterized by high
150 alkalinity (pH 9.7) and high salinity (TDS 4076 mg/L), according to the World Health Organization
151 (WHO) guideline for drinking water [33]. The dominant ions were Na⁺, SO₄²⁻, Cl⁻, and IC, including
152 CO₃²⁻ and HCO₃⁻. High levels of salinity and turbidity have no health significance, but they reduce
153 the acceptability of drinking water in terms of its taste, odor and appearance [33]. The F⁻ concentration
154 was 56.2 mg/L, which exceeded the WHO guideline of 1.5 mg/L by more than 37 times. Such high
155 level of F⁻ poses a genuine health risk of dental and skeletal fluorosis [25]. Therefore, F⁻, IC and EC
156 (represents salinity) were the three target components to treat in order to produce acceptable drinking
157 water from the Mdori brackish water.

158
159

160 Table 1 Water quality at Mdori borehole in northern Tanzania (GPS coordinates: S03°47.273',
 161 E035°51.138'), compared to WHO guidelines
 162

Parameter	Unit	Value	WHO guideline [33]
pH (25 °C)	–	9.7	6.5-8.5
EC (25 °C)	µS/cm	4940	–
TDS	mg/L	4076 ^a	1000 ^b
Turbidity	NTU	15.8	1 ^c
TOC	mg/L	5.3	–
IC	mg/L	430.0	–
F ⁻	mg/L	56.2	1.5
Cl ⁻	mg/L	268.0	250 ^b
SO ₄ ²⁻	mg/L	306.1	250 ^b
Al	mg/L	0.1	0.1 ^d
B	mg/L	1.9	2.4
Ca	mg/L	1.6	300 ^b
Fe	mg/L	0.2	0.3 ^b
K	mg/L	16.3	–
Mg	mg/L	0.5	–
Na	mg/L	1358.1	200 ^b
P	mg/L	0.7	–
Si	mg/L	17.3	–
Sr	mg/L	0.1	–

163 ^a Calculated as the sum of cations and anions, the charge difference between cations and anions < 5%.

164 ^b Based on average taste thresholds.

165 ^c Based on disinfection effectiveness.

166 ^d Based on optimization of the coagulation process.

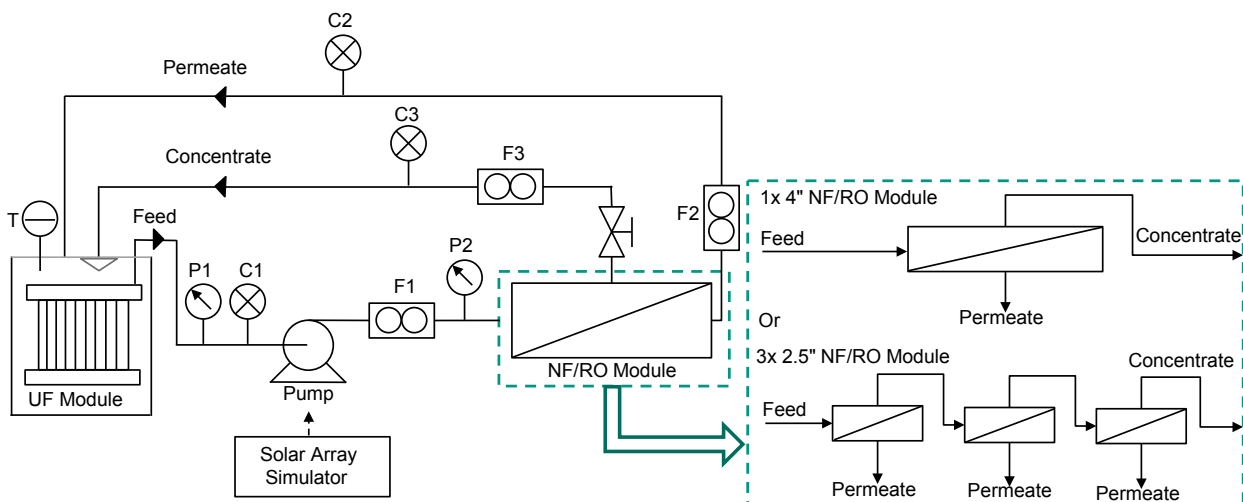
167 2.2. System design and membrane characteristics

168 An integrated PV-powered membrane system was used for the experiments. The filtration
 169 system combines ultrafiltration (UF) and NF/RO processes. The UF stage was used to remove
 170 particles, viruses and bacteria while the NF/RO stage was for desalination. A schematic is shown in
 171 Figure 1, while full details of the system have been published elsewhere [20, 34, 35]. As part of the
 172 design concept this system includes some unusual features; the system is operated at relatively low
 173 recovery (10-30%) and there is no energy recovery in the system (in form of a booster pump) that
 174 would enhance this recovery. The reason is firstly that very few suitable DC components exist to
 175 allow such operation for non-seawater systems. Secondly, provided the water is of such quality that

176 after the physical disinfection stage (UF) it can be safely used for washing or showering purposes,
 177 then this approach allows to avoid concentrate production. This is highly beneficial in remote areas
 178 where no adequate treatment of such concentrates is feasible. In this case this is indeed possible, as
 179 the feed water was used for laundry where fluoride is not a concern and the marginal increase in
 180 salinity can be tolerated.

181 The NF/RO elements were spiral wound in 40" (1 m) length and in two different diameters,
 182 2.5" and 4". Two different configurations, or modules, of the NF/RO elements were tested. The first
 183 module contained one 4" NF/RO element (denoted as the 1× 4" module), and the second module
 184 contained three 2.5" elements in series (denoted as the 3× 2.5" module) such that the concentrate of
 185 the first element became the feed to the second, and the concentrate of the second the feed of the
 186 third. Therefore, the length of the 3× 2.5" module was triple the length of the 1× 4" module, while
 187 the cross-sectional area of the 3× 2.5" module was approximately one-third of that of the 1× 4"
 188 module. In the 1× 4" module, the permeate and concentrate streams were recirculated into the feed
 189 tank; in the 3× 2.5" module, the three permeate streams (one from each element) and the concentrate
 190 stream of the last element were recirculated to the feed tank, separately. Pressure, temperature, flow
 191 rate and EC sensors were installed on the feed, permeate and concentrate streams. The sensor details
 192 can be found in a previous publication [35]. As the system was adapted to install the 3× 2.5" module
 193 in the existing system, no additional pressure sensors were added and hence the pressure drop across
 194 the individual modules is not available. This was exacerbated by the concentrate pressure sensor being
 195 not fully functional. These are a design and operational shortfalls that could not be remedied during
 196 the field work. Data from the sensors were recorded by a datalogger at 2 second intervals and
 197 transferred to a laptop using LabVIEW 8.0 software.

198



199

200

201 Figure 1 Schematic of the PV-powered membrane system configurations equipped with either 1× 4"
202 module or 3× 2.5" NF/RO module. Sensors are marked as T (temperature), P (pressure transducer),
203 C (EC) and F (flow).

204

205 Five types of NF/RO membrane, namely NF270, BW30, NF90, BW30LE and XLE (all
206 sourced from DOW Chemical, USA) were used. NF270 and NF90 are NF membranes while BW30,
207 BW30LE and XLE are brackish water RO membranes. Membrane specifications provided by the
208 manufacturer are summarized in Table 2. It is assumed that the membrane envelopes in both 2.5" and
209 4" elements have the same dimensions. The difference in their diameters are only due to different
210 numbers of envelopes that are wound into the 2.5" and 4" elements.

211

212 Table 2 Membrane specifications as provided by the manufacturer [36-42]

Type	Active area (m ²)	Permeance ^a (L/m ² .h.bar)	Retention (%)	Maximum feed flow (L/h)	Maximum pressure (bar)	Maximum recovery (%)
4" BW30	7.2	3.4	99.5 ^b	3600	41	90
2.5" BW30	2.6	3.3	99.5 ^b	1400	41	90
4" NF270	7.6	10.8	>97.0 ^c	3600	41	90
2.5" NF270	2.6	10.7	>97.0 ^c	1400	41	90
4" NF90	7.6	8.7	>97.0 ^c	3600	41	90
4" BW30LE	7.6	4.6	99.0 ^d	3600	41	90
2.5" XLE	2.6	7.4	99.0 ^e	1400	41	90

213 ^a Permeance (P) was calculate using the equation $P = \frac{Q_P}{A \times p}$, where Q_P was permeate flow at provided test conditions, p
214 is applied pressure and A is membrane active area.

215 ^b Test condition: 2000 mg/L NaCl at 15.5 bar, 15% recovery, 25 °C

216 ^c Test condition: 2000 mg/L MgSO₄ at 4.8 bar, 15% recovery, 25 °C

217 ^d Test condition: 2000 mg/L NaCl at 10.3 bar, 15% recovery, 25 °C

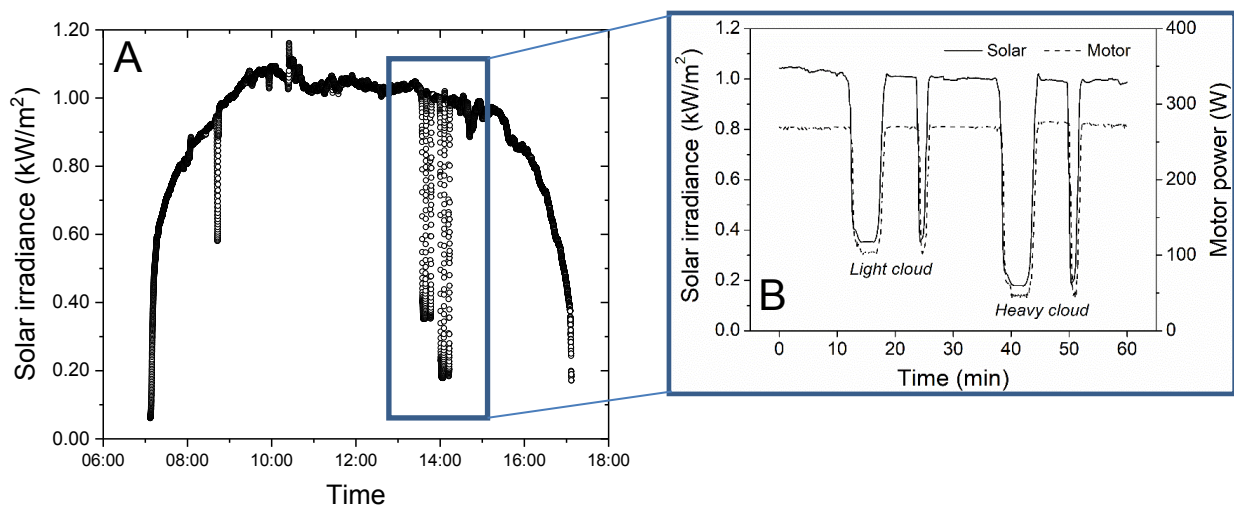
218 ^e Test condition: 500 mg/L NaCl at 6.9 bar, 15% recovery, 25 °C.

219

220 2.3. Experimental procedure

221 In order to have identical solar power quality for all experiments, a solar array simulator (SAS,
222 E4350B, Agilent Technologies, US) was used to power the helical rotor pump (Mono Sun-Sub,
223 Australia). When supplied with solar irradiance data, the SAS functions as a DC power supply that is
224 able to simulate the output of PV modules, thus enabling variable but repeatable solar conditions to
225 be investigated. The simulated PV modules are the ones actually mounted on the PV-membrane

226 system (BP Solar BP3150S, each provide a maximum power of 150 W). A 60-min period of solar
 227 irradiance data were recorded in a sunny day during the dry season in Tanzania. The solar irradiance
 228 and the resulting motor power of the pump are shown in Figure 2 in the context of the full day of
 229 solar irradiance (Figure 2A). The solar irradiance data in Figure 2B are characterized by three features:
 230 (i) the maximum intensity of about 1 kW/m², which occurs under cloudless skies; (ii) two short peaks
 231 of about 2 min duration occurring at $t = 24$ and $t = 50$ min with a minimum solar intensity of 0.36 and
 232 0.19 kW/m², respectively; and (iii) two longer duration peaks (6 to 7 min) at $t = 15$ and $t = 40$ with a
 233 minimum solar irradiance of 0.35 and 0.18 kW/m², respectively. These dips in solar irradiance occur
 234 due to passing clouds. From now on, peaks with 0.35 – 0.36 kW/m² intensity will be referred to as
 235 ‘light cloud period’ and peaks with 0.18 – 0.19 kW/m² intensity as ‘heavy cloud period’, as indicated
 236 in Figure 2. During the period of maximum intensity of solar irradiance (1 kW/m²) the power
 237 consumed by the pump was relatively constant at 270 W, which resulted in a constant pressure and
 238 feed flow in all experiments.
 239



240 Figure 2 Solar irradiance and the resulting motor power during (A) the full solar day with a controlled
 241 fluctuation and (B) the 60-min test period used for the experiments with different membranes and
 242 configurations

243
 244 As there was only one set of sensors in the permeate stream, it was impossible to
 245 simultaneously monitor the permeate stream of every element in the 3×2.5" module. Therefore, three
 246 repetitive experiments were conducted and in each experiment, one of the three permeate streams was
 247 connected to the sensors. Water samples from each permeate stream were manually collected every
 248 two minutes for further analyses. Prior to each experiment, the back-pressure valve was adjusted to a
 249 point where a similar feed flow was achieved at roughly the same pressure with different modules.
 250 The concept of such a “set-point” to enable fair comparison between different system configurations

251 was discussed in more detail in a previous paper [43]. The set-point for the different modules was
 252 chosen to be a pressure of 5.5 – 6.0 bar with a relatively low feed flow of 550 – 600 L/h. The following
 253 formulae were used to calculate the parameters to evaluate the performance of the system.

254

$$255 \quad R = \left(1 - \frac{C_P}{C_F}\right) \times 100\% \quad (1)$$

256

$$257 \quad Y = \left(\frac{Q_P}{Q_F}\right) \times 100\% \quad (2)$$

258

$$259 \quad \begin{aligned} J \\ = \frac{Q_P}{A} \end{aligned}$$

260 (3)

$$261 \quad SEC = \frac{I \times U}{Q_P} \quad (4)$$

262

$$263 \quad \begin{aligned} C_{3 \times 2.5} \\ = \frac{Q_{P1}C_{P1} + Q_{P2}C_{P2} + Q_{P3}C_{P3}}{Q_{P1} + Q_{P2} + Q_{P3}} \end{aligned} \quad (5)$$

264

$$265 \quad V_{cumulative} = \sum_{i=1}^t \left(\frac{Q_{Pi}}{1800}\right) \quad (6)$$

266

$$267 \quad \begin{aligned} C_{cumulative} \\ = \frac{\sum_{j=1}^t (C_{Pj} \times V_j)}{V_{cumulative}} \end{aligned} \quad (7)$$

268

269 In the above equations, C_F and C_P are the initial feed and permeate concentration (mg/L),
 270 respectively, Q_F and Q_P are the feed and permeate flow (L/h), respectively, R is retention (%), Y is
 271 recovery (%), J is flux (L/m².h), A is membrane active area (m²), SEC is specific energy consumption
 272 (kWh/m³), I is pump current (A), U is pump voltage (V), $C_{3 \times 2.5}$ is the fictitious permeate

273 concentration if three permeate streams of the $3 \times 2.5''$ module were merged (P1, P2, P3 refer to the
274 first, second and third permeate stream, repectively), $V_{cumulative}$ is the cumulative sum of permeate
275 water volume over time (L), $C_{cumulative}$ is the cumulative sum of permeate concentration over time
276 (mg/L). For each of the $2.5''$ elements, the SEC was calculated using $1/3$ of the motor power. To
277 calculate retention for the $2.5''$ elements, the original feed concentration, fed to the first element, was
278 considered as feed concentration for all three elements in the $3 \times 2.5''$ module. Pressure drop, expected
279 in the order of 0.03 to 0.15 bar per m (or in this case per element), was not monitored. This pressure
280 drop will be higher for the $3 \times 2.5''$ module due to i) a smaller cross-sectional area and hence higher
281 crossflow velocity, and ii) three modules in series.

282

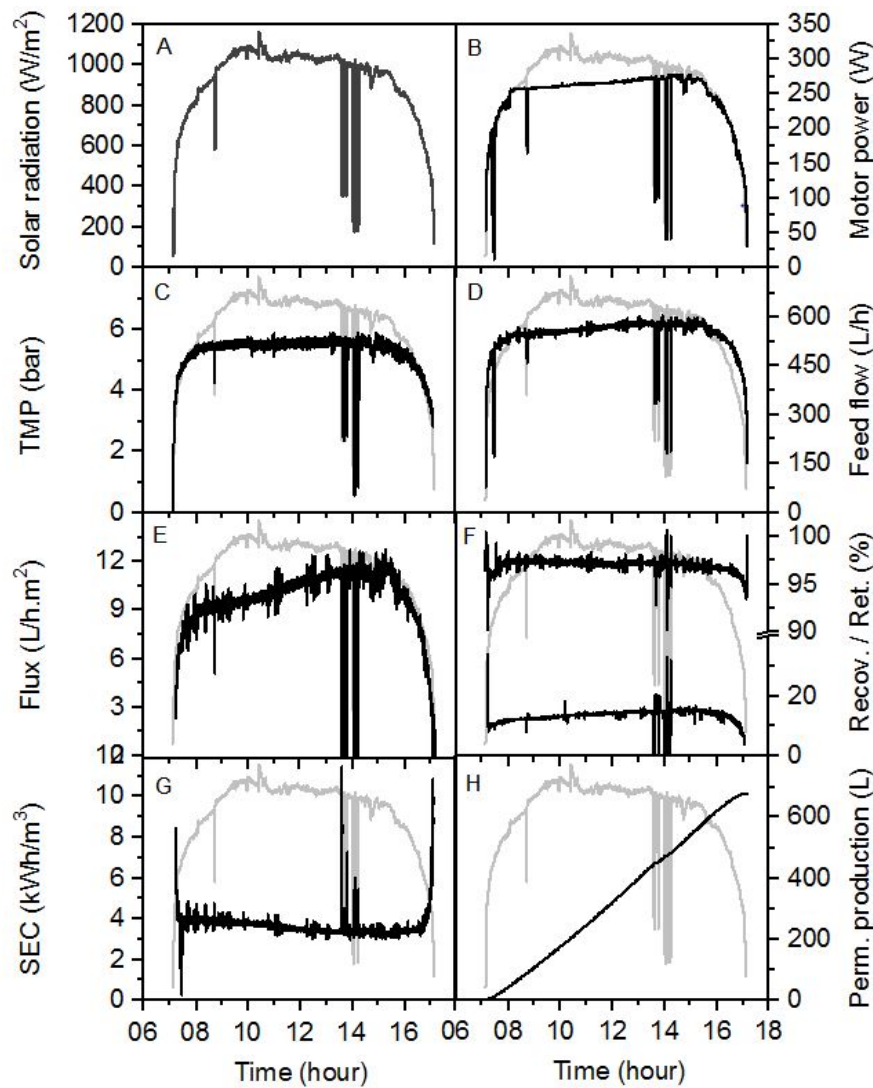
283 **3. Results & Discussion**

284 **3.1. Typical system performance over a solar day**

285 To set the work of different module configurations over the 60 min fluctuations period, a
286 typical result over a full day is shown in Figure 3 for the Mdori water and a 1× 4'' BW30 module. As
287 the sun rises in the morning (Figure 3A) the motor power (Figure 3B) is determined by the maximum
288 power point tracker and will drive the pump to provide the transmembrane pressure (TMP) (Figure
289 3C) and feed flow (Figure 3D). This results in a flux (Figure 3E) at a variable recovery and EC
290 retention (Figure 3F). Specific energy consumption (Figure 3G) can be calculated and ultimately the
291 amount of clean water (permeate) produced over such a solar day be determined (Figure 3F). Such
292 data was published previously with very detailed analysis for different waters [10] and for the same
293 water during field work [44] with a focus on transport mechanisms. The retention (in this graph that
294 of EC) varies with fluctuation because diffusion will play a significant role when the applied pressure
295 reduces. The same phenomena is typically observed for EC, IC and F.

296 Naturally the specific performance will change with membrane type, the main differences will
297 take place during the fluctuation where diffusion contributes disproportionately to permeate quality,
298 while during the maximum solar irradiation the performance of the membrane type can be deducted.
299 For this reason the further investigations are limited to this one hour fluctuation, taking very frequent
300 data readings. This results in a cumulative permeate volume of about 1/10th of a full solar day.

301



302

303 Figure 3 Typical full day experiment with Mdori water and 1×4'' module (BW30) with (A) Solar
 304 irradiance, (B) motor power, (C) transmembrane pressure (TMP), (D) feed flow, (E) flux, (F)
 305 recovery (*bottom*) and retention of electrical conductivity (*top*), (G) specific energy consumption
 306 (SEC), and (H) cumulative permeate production.

307 3.2. Performance of the 1×4'' and 3×2.5'' modules during cloudless periods

308 System performance under steady-state conditions was firstly studied as a point of reference
 309 for evaluating performance under fluctuating energy. The steady-state region was chosen to be
 310 between 34 and 36 min (Figure 2B). The results of NF270 and BW30 membranes in two module
 311 sizes (1×4'' and 3×2.5'') are presented in Table 3 and Table 4, respectively. The results of NF90,
 312 BW30LE and XLE membranes are presented in the Supplementary Information as Figure S2, S3, and
 313 S4, respectively.

314 Different modules of the same membrane obtained similar pressure and feed flow, confirming
 315 that the 'set-point' approach indeed provides a good basis for performance comparison. As shown in

316 Table 3, the 1× 4" module of NF270 produced permeate at a flux of 35.1 L/m².h and a recovery of
317 43.9%. The 3× 2.5" module of NF270 had a similar flux of 33.5 L/m² and a recovery of 49.3%. The
318 slightly larger difference in their recoveries was related to their different feed flows. The combined
319 SEC of the 3× 2.5" module was 0.98 kWh/m³, which was identical with that of the 1× 4" module.
320 When it comes to the individual elements, the flux and recovery decreased sharply from the first to
321 the third element. The flux decline was in general caused by a decreased net driving pressure and an
322 increased hydraulic resistance [45, 46]. The decrease of the net driving pressure was the result of (1)
323 the axial pressure drop along the feed channel, and (2) an increase in solute concentration and hence
324 in osmotic pressure due to water permeation and retention [23, 47]. The increased resistance included
325 (1) the friction resistance due to the prolonged flow path and (2) the local resistance when the
326 direction of flow was sharply changed (such as in endcaps and pipe bends) [23, 48, 49]. The SEC
327 increased from the first element to the third element accordingly.

328 Further, permeate EC, F⁻ and IC concentrations from the 3× 2.5" and 1× 4" modules of NF270
329 were compared (see Table 3). NF270 is known as a 'loose' NF membrane with a molecular weight
330 cut-off (MWCO) of 155 – 180 Da [31, 50]. NF270 rejects ions mainly based on charge repulsion [31,
331 51]. The permeate EC and IC of the 3× 2.5" module were both lower than that of the 1× 4" module.
332 This can be explained by the reduced concentration polarization in the 3× 2.5" module. Given that
333 the cross-sectional area of the 3× 2.5" module was only one-third of that of the 1× 4" module, the
334 crossflow velocity of the 3× 2.5" module was approximately triple that of the 1× 4" module at the
335 same feed flow. Therefore, the concentration polarization in the 3× 2.5" module was more reduced
336 by the higher crossflow velocity [52, 53]. A follow-up study using computational fluid dynamics has
337 revealed that the 3× 2.5" module had a lower wall concentration and a smaller boundary layer
338 thickness compared to the 1× 4" module [32]. Notably, the permeate F⁻ concentration of the 3× 2.5"
339 module was higher than those of the 1× 4" module. The negative effect of salinity and IC speciation
340 on F⁻ retention was attributed to charge screening and Donnan effect [51, 54, 55]. The permeate F⁻
341 concentrations of the 3× 2.5" and 1× 4" modules were both far beyond the WHO guideline of 1.5
342 mg/L and this membrane was clearly not suitable to produce potable water.

343 Within the 3× 2.5" module, the permeate concentrations increased sharply from the first
344 element to the third element. The permeate IC and F⁻ from the third element were approximately
345 doubled as compared with those from the first element. Such rapid degradation of permeate quality
346 was attributed to: (1) the increased feed concentration from first to third element; and (2) the
347 decreased net driving pressure due to the axial pressure drop and the increased osmotic pressure.

348

349 Table 3 Summary of performance indicators of the 1× 4" and 3× 2.5" modules of NF270 under steady-
 350 state operation during cloudless periods (1 kW/m² solar irradiance).

	1× 4 "module	3× 2.5 "module			
		Combined	First element	Second element	Third element
Flux (L/m ² .h)	35.1	33.5	42.2	30.7	27.7
Recovery (%)	43.9	49.3	20.7	15.0	13.6
SEC (kWh/m ³)	0.98	0.98	0.82	1.12	1.25
Permeate EC (μS/cm)	2012.3	1881.5	1554.6	1779.6	2492.3
Permeate F ⁻ (mg/L)	25.9	30.2	20.6	30.5	44.4
Permeate IC (mg/L)	176	154	107	154	227

351
 352 Not surprisingly, when comparing the performance of BW30 to NF270, the former exhibited
 353 a noticeably lower flux and higher SEC, but produced permeate with a higher quality (Table 4). The
 354 flux of the 1× 4" module of BW30 was 11.7 L/m².h, while the combined permeate flux of the 3× 2.5"
 355 module was 8.2 L/m².h. The lower flux of the 3× 2.5" module was because of a higher axial pressure
 356 drop (a lower net driving pressure) and a higher hydraulic resistance along the feed channel. This is
 357 due to the 3× 2.5" module being three times as long as the 1× 4" module as well as the higher velocity,
 358 even though the higher velocity is expected to reduce concentration polarization. Furthermore, the
 359 difference in flux between two modules was more significant for BW30 over NF270 due to a higher
 360 rejection and hence higher osmotic pressure difference resulting in a lower net driving pressure.
 361 Therefore the axial pressure drop probably had a bigger impact on BW30 than on NF270. The SEC
 362 of the 3× 2.5" module (4.24 kWh/m³) was higher than that of the 1× 4" module (3.21 kWh/m³) as a
 363 result of the lower flux. As a 'tight' RO membrane (MWCO 98 Da [50]), BW30 rejects ions primarily
 364 based on size exclusion [31]. The permeate EC of the 3× 2.5" module was lower than that of the 1×
 365 4" module, which suggests that the 3× 2.5" module was better than the 1× 4" module in rejecting total
 366 dissolved salts. However, the permeate F⁻ and IC concentrations of the 3× 2.5" module were slightly
 367 higher than those of the 1× 4" module. A possible explanation is that F⁻ and IC (*i.e.* CO₃²⁻ and HCO₃⁻)
 368 in the 3× 2.5" module were less retained than other larger anions that contributed to EC (such as Cl⁻
 369 and SO₄²⁻) by size exclusion [56, 57]. Noticeably, both modules managed to reduce the permeate F⁻
 370 concentration to meet the WHO guideline of 1.5 mg/L, even for the third element of the 3× 2.5"
 371 module.

372

373 Table 4 Summary of performance indicators of the 1× 4" and 3× 2.5" modules of BW30 under steady-
 374 state operation during cloudless periods (1 kW/m² solar irradiance).

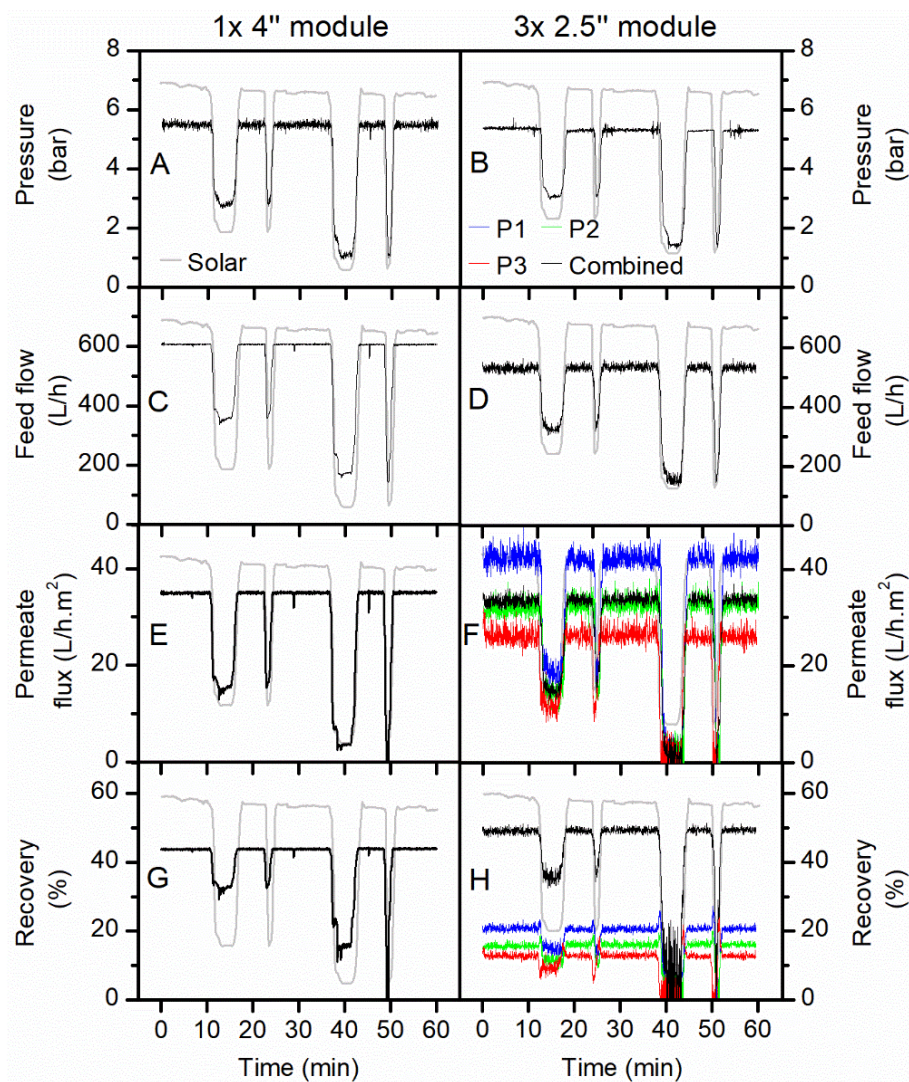
	1× 4 "module	3× 2.5 "module			
		Combined	First element	Second element	Third element
Flux (L/m ² .h)	11.7	8.2	10.9	9.4	4.2
Recovery (%)	14.4	11.4	5.1	4.4	1.9
SEC (kWh/m ³)	3.21	4.24	3.17	3.68	8.28
Permeate EC (μS/cm)	134.6	57.5	34.6	63.7	103.5
Permeate F ⁻ (mg/L)	0.5	0.8	0.6	0.8	1.2
Permeate IC (mg/L)	3.1	5.4	4.1	5.5	8.5

375

376 **3.3. Performance of the 1× 4" and 3× 2.5" modules of NF270 during cloudy periods**

377 The instantaneous performance of the 1× 4" and 3× 2.5" modules of the loose NF membrane
 378 NF270 are presented in Figure 4 and Figure 5, respectively. During the light and heavy cloud periods,
 379 the pressure and feed flow decreased sharply due to significant reduction in input power. For the 1×
 380 4" module, when the solar irradiance dropped from 1 to 0.2 kW/m² at 50 min, the pressure reduced
 381 from 5.5 to 0.9 bar and the feed flow reduced from 600 to 130 L/h (refer Figure 4A, C). The flux
 382 therefore decreased from 35 L/m².h to 0 L/m².h due to insufficient power (see Figure 4E), while the
 383 recovery dropped from 44% to 0% accordingly (see Figure 4G). As for the 3× 2.5" module, the
 384 variations of pressure and feed flow were very similar to those of the 1× 4" module, except that the
 385 feed flow was slightly lower (about 10%) than that of the 1× 4" module (see Figure 4B and D). The
 386 lower feed flow of the 3× 2.5" module was probably due to the increased hydraulic resistance. The
 387 fluxes – not only the flux from individual element but also the combined flux calculated from total
 388 permeate volume and total membrane area – dropped sharply during the light and heavy cloud periods
 389 and decreased to 0 L/m².h at 42 and 50 min (Figure 4F). The combined flux of the 3× 2.5" module
 390 was equal to the flux of the 1× 4" module. The recovery varied with the feed flow and permeate flux
 391 (Figure 4H). The combined recovery of the 3× 2.5" module, which equals to the sum of individual
 392 recoveries of each element, was slightly higher than the 1× 4" module because of its lower feed flow.

393



394
 395 Figure 4 Comparison of the 1× 4" and 3× 2.5" modules of NF270 over 60 min of the solar day: (A,
 396 B) pressure, (C, D) feed flow, (E, F) flux, (G, H) recovery.

397
 398 Notably, unstable readings were observed in feed flow and flux of the 3× 2.5" module. In
 399 order to maximize the use of space in the PV-powered membrane system, the three elements in series
 400 were arranged vertically from top to bottom. Consequently, the pipes connecting adjacent elements
 401 were sharply curved, which caused flow disturbances and thus affected flow measurement [58, 59].
 402 In addition, the tripled length of the flow path, the nearly tripled crossflow velocity, and the excessive
 403 number of endcaps in the 3× 2.5" module could also contribute to the unstable flow readings.
 404 Nevertheless, such unstable readings could be tolerated since they did not shield the measurement
 405 under fluctuating solar conditions, which was the specific focus of this study.

406 The results of the SEC and permeate quality produced by the two modules of NF270 are
 407 presented in Figure 5. The SEC mainly depends on the salinity of the water, the permeability of the
 408 membrane, the configuration of the system, the recovery, and the efficiency of the pump [60, 61].

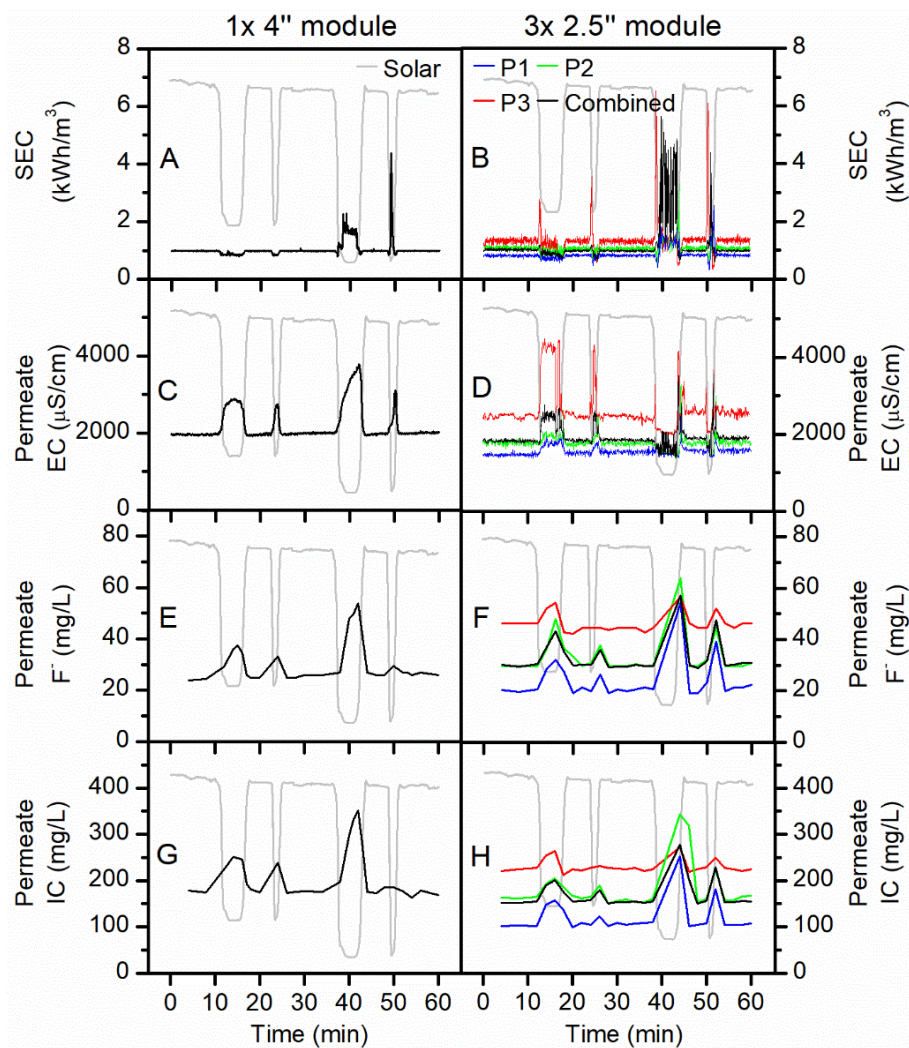
409 There was no markedly difference between the combined SEC of the 3× 2.5" module and the SEC of
410 the 1× 4" module under maximum intensity of solar irradiance. However, the SEC of the 3× 2.5"
411 modules demonstrated more dramatic volatility during the heavy cloud periods, which were attributed
412 to greater variations in the flux values (Figure 5B).

413 The 1× 4" module showed an increase in EC from 2000 to 3000 $\mu\text{S}/\text{cm}$ during the light cloud
414 period and from 2000 to 4000 $\mu\text{S}/\text{cm}$ during the heavy cloud period (Figure 5C). The increased salt
415 concentration during cloudy periods was primarily attributed to the severe drop in flux resulting in
416 less 'dilution'. Besides, the decline in feed flow reduced the crossflow velocity and thus probably
417 facilitated salt diffusion across the membrane [10]. In the 3× 2.5" module, the effect of energy
418 fluctuation on permeate EC was drastic for the third element while the effect was rather moderate for
419 the first two elements. As the available solar irradiance decreased from 1000 to 350 W/m^2 , during the
420 light cloud period, the permeate EC of the first element increased slightly from 1400 to 1800 $\mu\text{S}/\text{cm}$,
421 while the third element experienced a drastic increase from 2500 to 4500 $\mu\text{S}/\text{cm}$ (Figure 5D). During
422 the heavy cloud period, the flux reached 0 $\text{L}/\text{m}^2\cdot\text{h}$. The peak appearing at the end of the heavy cloud
423 period was due to the washing away of permeate that remained in the system during this downtime.

424 The permeate F^- and IC of both modules varied with solar irradiance in an analogous manner,
425 which exhibited an abrupt peak during the heavy cloud period (Figure 5E–H). This was again because
426 of the severe flux reduction. It is worthwhile mentioning that the permeate F^- and IC of the third
427 element of the 3× 2.5" module appears to be less affected by energy fluctuation, which seems
428 inconsistent with the trend of the permeate EC. This is in fact due to the two different measurement
429 methods of EC and F^-/IC , namely in-line monitoring and manual water sampling [62]. The permeate
430 EC was measured continuously by the in-line EC sensor, thereby the EC peaks were precisely
431 recorded. The permeate F^- and IC concentration, on the other hand, were measured intermittently
432 from discrete samples (samples were taken every two minutes). Inevitably there was some
433 unavoidable error in the peak positions and amplitudes.

434 Considering the flux, SEC and permeate quality, the performance of the first element of the
435 3× 2.5" module was better than the 1× 4" module. However, the deficient performance of the third
436 element of the 3× 2.5" module resulted in obtaining a similar overall performance compared to the
437 1× 4" module.

438



439

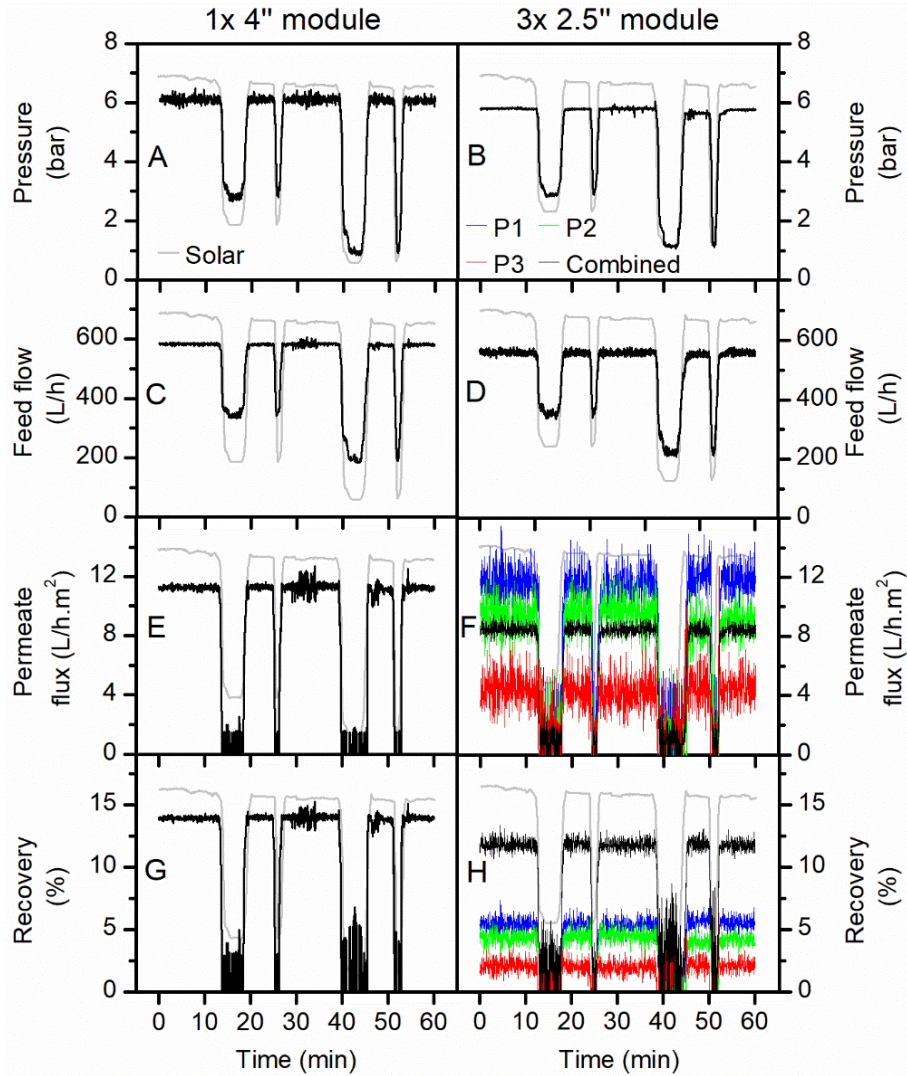
440 Figure 5 Comparison of the 1× 4'' and 3× 2.5'' modules of NF270 over 60 min of the solar day: (A,
 441 B) SEC, (C, D) permeate EC, (E, F) permeate F⁻ concentration, (G, H) permeate IC concentration.

442

443 3.4. Performance of the 1× 4'' and 3× 2.5'' modules of BW30 during cloudy periods

444 The effect of changing to a denser SW membrane with high salt retention, BW30, on the
 445 performance of the batteryless PV-powered system was studied as well. The results of the
 446 performance testing of the two configurations, 1× 4'' and 3× 2.5'' BW30 modules, are presented in
 447 Figure 6 and Figure 7. The pressure applied to both BW30 module types were nearly identical, as
 448 were the feed flows (Figure 6A–D). The unstable readings in feed flow and flux of the 3× 2.5'' module
 449 under steady-state conditions were attributed to flow disturbances, as explained earlier for NF270.
 450 Flux and recovery of the 1× 4'' module of BW30 was notably better than the 3× 2.5'' module (Figure
 451 6E–H), which was attributed to a lower axial pressure drop and a lower hydraulic resistance. In
 452 consequence, the combined SEC of the 3× 2.5'' module was higher than that of the 1× 4'' module, let
 453 alone the extremely high SEC of the third element of the 3× 2.5'' module (Figure 7A,B). As discussed

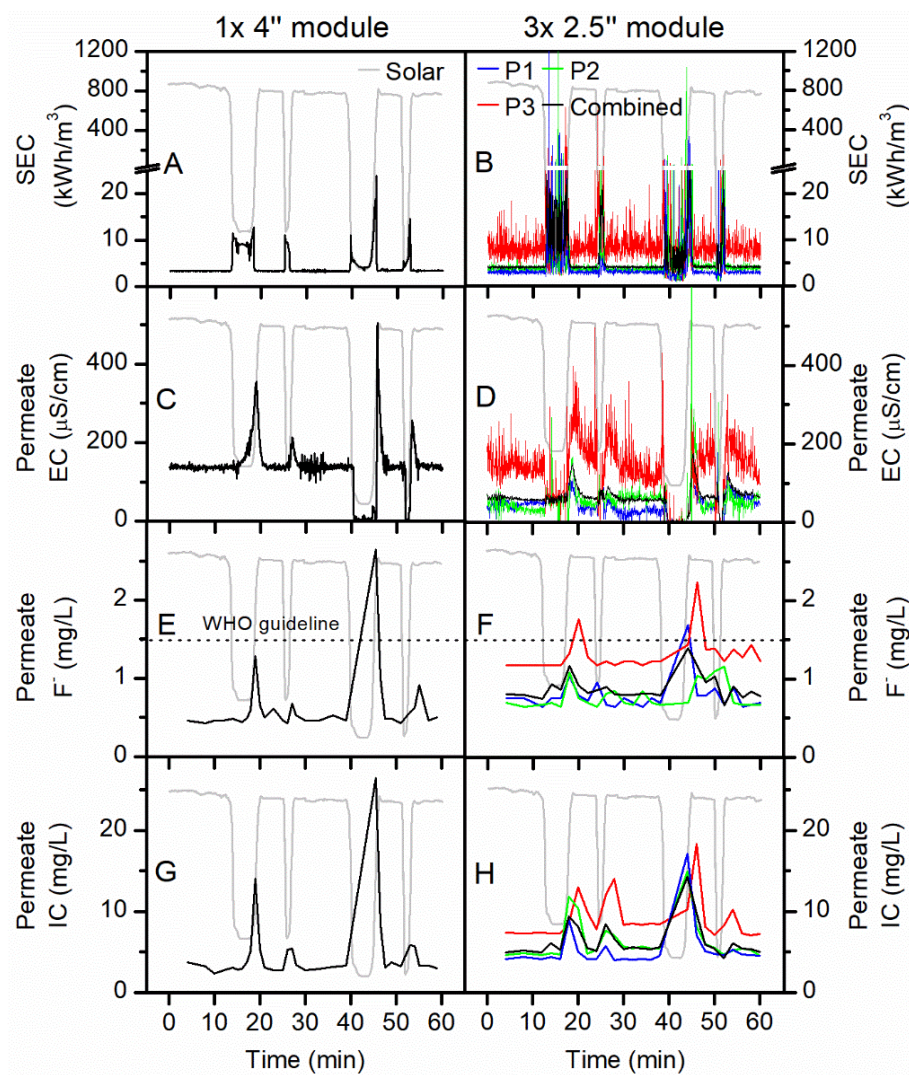
454 above, the higher rejecting BW30 was more sensitive to axial pressure drop than the NF270 because
455 of a higher osmotic pressure and thus a lower net driving pressure. Therefore the 3× 2.5" module
456 performed more poorly compared to the 1× 4" module when using BW30.
457



458
459 Figure 6 Comparison of the 1× 4" and 3× 2.5" modules of BW30 over 60 min of the solar day: (A,
460 B) pressure, (C, D) feed flow, (E, F) flux, (G, H) recovery.

461
462 It is noteworthy that the flux values of both modules dropped to 0 L/m².h during the light and
463 heavy cloud periods, which had a negative impact on the permeate quality. There was a spike in the
464 permeate EC upon the end of every cloud period. The zero permeate EC reading during the heavy
465 cloud period was because of air in the sensor (Figure 7C,D). The combined permeate EC of the 3×
466 2.5" module was lower than that of the 1× 4" module, due to the first and third elements of the 3×
467 2.5" module exhibiting remarkably efficient salt rejection (Figure 7D). In contrast, the third element
468 of the 3× 2.5" module performed rather poorly in this respect.

469 Regarding F^- and IC removal, the performance of $1 \times 4''$ module was better than the $3 \times 2.5''$
 470 module (Figure 7E–H). When analyzing individual elements of the $3 \times 2.5''$ module, the first two
 471 elements of the $3 \times 2.5''$ module exhibited good removal efficiency while the third element was
 472 inefficient in this regard. In fact, the performance of the third element was so poor that it was hardly
 473 worth having this element present in the module. It is noteworthy that the permeate F^- concentration
 474 of both modules temporarily exceeded the guideline value during the cloud periods. However, when
 475 considering that the permeate was continuously stored in a product tank, the system equipped with
 476 BW30 modules was able to produce safe drinking water in a long term, as will be discussed below.
 477



478
 479 Figure 7 Comparison of the $1 \times 4''$ and $3 \times 2.5''$ modules of BW30 over 60 min of the solar day: (A,
 480 B) SEC, (C, D) permeate EC, (E, F) permeate F^- concentration, (G, H) permeate IC concentration.
 481

482 3.5. Overall comparison of the 1×4" and 3×2.5" modules

483 As discussed above, the performance of the 1×4" and 3×2.5" modules of the NF270 and
484 BW30 membranes were evaluated and compared respectively during both cloudless and cloudy
485 periods. The overall performances of these modules were characterized by two parameters: the first
486 parameter is the cumulative sum of permeate water volume over time, which represents the
487 productivity of the module; the second parameter is the cumulative sum of permeate F⁻ concentration
488 over time, which indicates the permeate quality when continuously collected in a tank. The results
489 are shown in Figure 8, along with the results for two other 1×4" modules (NF90 and BW30LE) and
490 one 3×2.5" module (XLE), for which the complete performance data are presented in the
491 Supplementary Information. The flux for the first two 2.5" elements is higher than the flux for the
492 4" element, while permeate F⁻ concentration of the 2.5" elements is higher (2 mg/L) than that of the
493 4" inch element (<1 mg/L). This is somewhat anomalous and because the XLE membrane is not
494 usually included in this research no clear explanation for observation can be provided. Possibly this
495 performance is due to a quality variation between the individual elements.

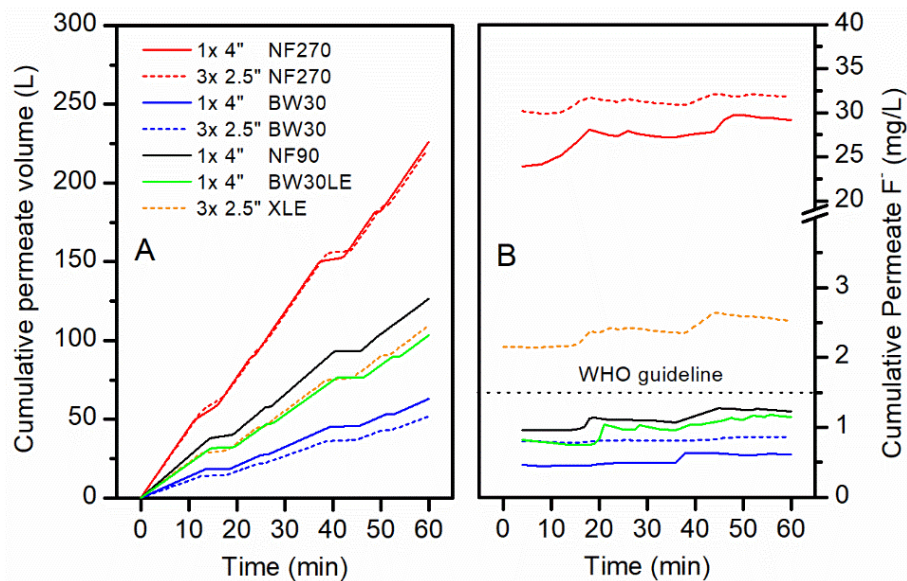
496 The cumulative permeate volume of all modules increased linearly with time, apart from
497 during the cloud periods when the productivity was reduced for a short time (Figure 8A). In case of
498 NF270, the permeate volumes produced by both modules were nearly the same (222 – 226 L),
499 whereas for BW30 the 1×4" module (63 L) produced a higher permeate volume than the 3×2.5"
500 module (52 L). The other three modules contained tight NF (NF90) and low energy RO (BW30LE,
501 XLE) membranes. Their water productivities were around halfway between that of the loose NF
502 (NF270) and the tight RO (BW30) membranes. The overall order was as follows: 1×4" NF270 > 3×
503 2.5" NF270 > 1×4" NF90 > 3×2.5" XLE > 1×4" BW30LE > 1×4" BW30 > 3×2.5" BW30, which
504 was completely consistent with the order of the permeance values, as reported in Table 2.

505 The cumulative permeate F⁻ concentration of all modules increased in a stepped manner due
506 to the dramatic soar of transient concentration during the cloud periods (Figure 8B). It is evident that
507 the 1×4" module had a better performance than the 3×2.5" module for both NF270 and BW30. As
508 discussed above, the third element of the 3×2.5" module reduced the overall performance of the
509 module significantly, which was due to the increasing feed concentration and the greater pressure
510 drop along the feed channel. The cumulative permeate F⁻ concentration of all modules followed the
511 order: 3×2.5" NF270 > 1×4" NF270 > 3×2.5" XLE > 1×4" NF90 > 1×4" BW30LE > 3×2.5"
512 BW30 > 1×4" BW30. The order of membrane type was in good agreement with the salt rejection
513 data provided by the manufacturer [63]. Even though the cloudy periods did not contribute
514 substantially to water quality in this study, when longer cloud periods are experienced and

515 consequently the transients are even longer this contribution may need to be controlled to not
516 compromise the overall water quality. Long term tests will be required to evaluate this and the control
517 algorithm and hardware may be expanded to include a permeate flush for such periods.

518 When referring to the WHO guideline limit for F^- concentration of 1.5 mg/L, three 1× 4"
519 modules (1× 4" BW30, 1× 4" BW30LE and 1× 4" NF90) and one 3× 2.5" module (3× 2.5" BW30)
520 were able to meet the guideline throughout the 60-min period. The other three modules (3× 2.5"
521 NF270, 1× 4" NF270, and 3× 2.5" XLE), on the contrary, failed to produce permeate with acceptable
522 F^- concentrations. It should be noted that XLE, as a RO membrane, was designed to have a higher
523 salt rejection than NF90 [63]. The inferior F^- removal of 3× 2.5" XLE compared to 1× 4" NF90
524 revealed the significant impact of module size on the actual system performance. The 1× 4" NF90
525 module seemed to be the best option in balancing permeate productivity and quality, which produced
526 127 L of drinking water with 1.2 mg/L F^- within the 60-min period.

527 When it comes to the cost factor, the market price of three 2.5" elements is much higher than
528 that of one 4" element, let alone the extra associated costs for three elements, such as extra tubing and
529 pressure vessels. It is thus more cost-effective to use the 1× 4" module rather than the 3× 2.5" module.
530



531
532 Figure 8 Comparison of cumulative (A) permeate volume and (B) permeate F^- concentration for
533 different 1× 4" and 3× 2.5" modules over 60 min of the solar day.
534

535 4. Conclusions

536 This study investigated the impact of membrane module size on the performance of a
537 batteryless PV-powered membrane system under fluctuating solar conditions. Several NF/RO

538 membranes in two module sizes ($1 \times 4''$ and $3 \times 2.5''$) of the same membrane area were used to treat a
539 naturally fluoridated brackish water in a remote village in northern Tanzania.

540 Under steady-state conditions, the $1 \times 4''$ and $3 \times 2.5''$ modules of NF270 achieved good flux
541 ($33 - 35 \text{ L/m}^2\cdot\text{h}$) and SEC (0.98 kWh/m^3), but as expected, the permeate quality ($25 - 30 \text{ mg/L F}^-$)
542 was too poor to meet the drinking water guideline for fluoride. Meanwhile the $1 \times 4''$ and $3 \times 2.5''$
543 modules of BW30 exhibited much lower flux ($8 - 12 \text{ L/m}^2\cdot\text{h}$) and correspondingly a higher SEC (3
544 $- 4 \text{ kWh/m}^3$), but the permeate F^- concentration ($0.5 - 0.8 \text{ mg/L}$) was satisfactory for drinking
545 purposes.

546 Under fluctuating solar conditions, the pressure and feed flow of the modules decreased
547 drastically, thus reducing the flux and increasing the SEC. The permeate water quality degraded
548 sharply because of the severe drop in flux. The transient permeate F^- concentration of BW30 modules
549 temporarily exceeded the guideline value. However, if being collected in a product tank, the
550 cumulative permeate F^- concentration of BW30 could always meet the WHO drinking water
551 guideline. The NF90 and BW30LE modules also achieved very good performance.

552 The performance of the $1 \times 4''$ module was always equivalent to or better than that of the $3 \times$
553 $2.5''$ module of the same membrane. This was mainly because the third element of the $3 \times 2.5''$ module
554 decreased the overall performance of the module substantially. Taking into account the cost factor,
555 large diameter SW modules enable considerable reductions in capital cost and life-cycle cost, thereby
556 increasing the economic feasibility of implementing PV-powered membrane systems in remote and
557 rural locations. Future work will focus on development of appropriate modelling frameworks for
558 performance simulation of PV-powered membrane systems during both steady-state and fluctuating
559 operations.

560

561 **5. Acknowledgements**

562 The research was funded in part by two Leverhulme Royal Society Africa Awards SADWAT-
563 Tanzania and SUCCESS; as well as the Helmholtz Association Recruitment Initiative for AIS and
564 BSR. The Energy Technology Partnership (ETP) and Drinking Water Quality Regulator for Scotland
565 (DWQR) provided the PhD scholarship for JS. The DOW Chemical Company kindly donated the
566 NF/RO membrane modules for this project, and GE Power & Water (Zenon) the UF module. Godfrey
567 Mkongo (Ngurdoto Defluoridation Research Station (NDRS), Tanzania) is greatly appreciated for his
568 hospitality when carrying out experiments at NDRS. William Dahi (Defluoridation Technology
569 Project, Tanzania) carried out the analysis of a huge number of samples, while Elly Karle and
570 Reinhard Sembritzki (KIT, Germany) provided IC and ICP data the source water sample. Minh

571 Nguyen (KIT, Germany) is thanked for drawing the graphic of the spiral wound element in the SI.
572 Prof Jack Gilron (BGU, Israel) has inspired this work through his questions at the PhD defense of
573 Gavin Park.
574

575 **6. Supplementary Information**

576 The SI contains a schematic of a spiral wound module, as well as further data of the NF90,
577 BW30LE and XLE membranes.

578 **7. References**

579 [1] J. Alcamo, N. Fernandez, S.A. Leonard, P. Peduzzi, A. Singh, R. Harding Rohr Reis, 21 issues
580 for the 21st Century: results of the UNEP Foresight Process on Emerging Environmental issues,
581 (2012).

582 [2] B.S. Richards, J. Shen, A.I. Schäfer, Water–energy nexus perspectives in the context of
583 photovoltaic-powered decentralized water treatment systems: A Tanzanian case study, *Energy*
584 *Technology*, (2017) 1-13.

585 [3] A.I. Schäfer, A. Broeckmann, B.S. Richards, *Renewable Energy Powered Membrane Technology*.
586 1. Development and Characterization of a Photovoltaic Hybrid Membrane System, *Environmental*
587 *Science & Technology*, 41 (2007) 998-1003.

588 [4] V.G. Gude, N. Nirmalakhandan, S. Deng, Renewable and sustainable approaches for desalination,
589 *Renewable and Sustainable Energy Reviews*, 14 (2010) 2641-2654.

590 [5] M. Shatat, M. Worall, S. Riffat, Opportunities for solar water desalination worldwide: Review,
591 *Sustainable Cities and Society*, 9 (2013) 67-80.

592 [6] D. Herold, A. Neskakis, A small PV-driven reverse osmosis desalination plant on the island of
593 Gran Canaria, *Desalination*, 137 (2001) 285-292.

594 [7] M. Thomson, D. Infield, A photovoltaic-powered seawater reverse-osmosis system without
595 batteries, *Desalination*, 153 (2003) 1-8.

596 [8] A. Chafidz, E.D. Kerme, I. Wazeer, Y. Khalid, A. Ajbar, S.M. Al-Zahrani, Design and fabrication
597 of a portable and hybrid solar-powered membrane distillation system, *Journal of Cleaner Production*,
598 133 (2016) 631-647.

599 [9] S.M. Shalaby, Reverse osmosis desalination powered by photovoltaic and solar Rankine cycle
600 power systems: A review, *Renewable and Sustainable Energy Reviews*, 73 (2017) 789-797.

601 [10] J. Shen, B.S. Richards, A.I. Schäfer, Renewable energy powered membrane technology: Case
602 study of St. Dorcas borehole in Tanzania demonstrating fluoride removal via nanofiltration/reverse
603 osmosis, *Separation and Purification Technology*, 170 (2016) 445-452.

604 [11] A. Joyce, D. Loureiro, C. Rodrigues, S. Castro, Small reverse osmosis units using PV systems
605 for water purification in rural places, *Desalination*, 137 (2001) 39-44.

- 606 [12] T. Espino, B. Peñate, G. Piernavieja, D. Herold, A. Neskakis, Optimised desalination of seawater
607 by a PV powered reverse osmosis plant for a decentralised coastal water supply, *Desalination*, 156
608 (2003) 349-350.
- 609 [13] M.A. Alghoul, P. Poovanaesvaran, M.H. Mohammed, A.M. Fadhil, A.F. Muftah, M.M. Alkilani,
610 K. Sopian, Design and experimental performance of brackish water reverse osmosis desalination unit
611 powered by 2 kW photovoltaic system, *Renewable Energy*, 93 (2016) 101-114.
- 612 [14] B.S. Richards, D.P.S. Capão, A.I. Schäfer, Renewable energy powered membrane technology.
613 2. The effect of energy fluctuations on performance of a photovoltaic hybrid membrane system,
614 *Environmental Science & Technology*, 42 (2008) 4563-4569.
- 615 [15] E.S. Mohamed, G. Papadakis, E. Mathioulakis, V. Belessiotis, A direct coupled photovoltaic
616 seawater reverse osmosis desalination system toward battery based systems — a technical and
617 economical experimental comparative study, *Desalination*, 221 (2008) 17-22.
- 618 [16] M. Thomson, D. Infield, Laboratory demonstration of a photovoltaic-powered seawater reverse-
619 osmosis system without batteries, *Desalination*, 183 (2005) 105-111.
- 620 [17] B.S. Richards, D.P.S. Capão, W.G. Früh, A.I. Schäfer, Renewable energy powered membrane
621 technology: Impact of solar irradiance fluctuations on performance of a brackish water reverse
622 osmosis system, *Separation and Purification Technology*, 156, Part 2 (2015) 379-390.
- 623 [18] L.A. Richards, B.S. Richards, A.I. Schäfer, Renewable energy powered membrane technology:
624 Salt and inorganic contaminant removal by nanofiltration/reverse osmosis, *Journal of Membrane
625 Science*, 369 (2011) 188-195.
- 626 [19] Dow Water and Process Solutions, FILMTEC™ Reverse Osmosis Membranes Technical
627 Manual,
628 http://msdssearch.dow.com/PublishedLiteratureDOWCOM/dh_095b/0901b8038095b91d.pdf?filepath=/609-00071.pdf&fromPage=GetDoc. Access date: May.
629
- 630 [20] J. Shen, G. Mkongo, G. Abbt-Braun, S.L. Ceppi, B.S. Richards, A.I. Schäfer, Renewable energy
631 powered membrane technology: Fluoride removal in a rural community in northern Tanzania,
632 *Separation and Purification Technology*, 149 (2015) 349-361.
- 633 [21] J. Schwinge, P.R. Neal, D.E. Wiley, D.F. Fletcher, A.G. Fane, Spiral wound modules and spacers:
634 Review and analysis, *Journal of Membrane Science*, 242 (2004) 129-153.
- 635 [22] A.J. Karabelas, M. Kostoglou, C.P. Koutsou, Modeling of spiral wound membrane desalination
636 modules and plants – review and research priorities, *Desalination*, 356 (2015) 165-186.
- 637 [23] J. Johnson, M. Busch, Engineering aspects of reverse osmosis module design, *Desalination and
638 Water Treatment*, 15 (2010) 236-248.
- 639 [24] A.J. Karabelas, C.P. Koutsou, M. Kostoglou, The effect of spiral wound membrane element
640 design characteristics on its performance in steady state desalination — A parametric study,
641 *Desalination*, 332 (2014) 76-90.
- 642 [25] J. Fawell, K. Bailey, J. Chilton, E. Dahi, L. Fewtrell, Y. Magara, Fluoride in drinking water,
643 World Health Organization, London 2006.

- 644 [26] J.P. Shorter, J. Massawe, N. Parry, R.W. Walker, Comparison of two village primary schools in
645 northern Tanzania affected by fluorosis, *International Health*, 2 (2010) 269-274.
- 646 [27] H.G. Jarvis, P. Heslop, J. Kisima, W.K. Gray, G. Ndossi, A. Maguire, R.W. Walker, Prevalence
647 and aetiology of juvenile skeletal fluorosis in the south-west of the Hai district, Tanzania – a
648 community-based prevalence and case-control study, *Tropical Medicine & International Health*, 18
649 (2013) 222-229.
- 650 [28] H. Mjengera, G. Mkongo, Appropriate defluoridation technology for use in flourotic areas in
651 Tanzania, *Physics and Chemistry of the Earth*, 28 (2003) 1097-1104.
- 652 [29] S. Ayoob, A.K. Gupta, V.T. Bhat, A conceptual overview on sustainable technologies for the
653 defluoridation of drinking water, *Critical Reviews in Environmental Science and Technology*, 38
654 (2008) 401-470.
- 655 [30] K.M.K. Kut, A. Sarswat, A. Srivastava, C.U. Pittman, D. Mohan, A review of fluoride in african
656 groundwater and local remediation methods, *Groundwater for Sustainable Development*, 2-3 (2016)
657 190-212.
- 658 [31] J. Shen, A.I. Schäfer, Factors affecting fluoride and natural organic matter (NOM) removal from
659 natural waters in Tanzania by nanofiltration/reverse osmosis, *Science of The Total Environment*,
660 527–528 (2015) 520-529.
- 661 [32] C. Onorato, M. Gaedtke, M. Kespe, H. Nirschl, A.I. Schäfer, Renewable energy powered
662 membrane technology: computational fluid dynamics evaluation of system performance with variable
663 module size and fluctuating energy, *Separation and Purification Technology*, (2019).
- 664 [33] World Health Organization, Guidelines for drinking-water quality: fourth edition incorporating
665 the first addendum, in, Geneva, 2017.
- 666 [34] A.I. Schäfer, A. Broeckmann, B.S. Richards, Renewable energy powered membrane technology.
667 1. development and characterization of a photovoltaic hybrid membrane system, *Environmental
668 Science & Technology*, 41 (2006) 998-1003.
- 669 [35] B.S. Richards, G.L. Park, T. Pietzsch, A.I. Schäfer, Renewable energy powered membrane
670 technology: Brackish water desalination system operated using real wind fluctuations and energy
671 buffering, *Journal of Membrane Science*, 468 (2014) 224-232.
- 672 [36] Dow Chemical Company, DOW FILMTEC Fibreglassed Elements for Light Industrial Systems,
673 <http://www.dupont.com/content/dam/Dupont2.0/Products/water/literature/609-00350.pdf>. Access
674 date: 12 November 2018.
- 675 [37] Dow Chemical Company, FILMTEC Membranes NF270 Nanofiltration Elements for
676 Commercial Systems,
677 <http://www.dupont.com/content/dam/Dupont2.0/Products/water/literature/609-00519.pdf>. Access
678 date: 12 November 2018.
- 679 [38] Dow Chemical Company, DOW FILMTEC Membranes DOW FILMTEC NF90 Nanofiltration
680 Elements for Commercial Systems,
681 <http://www.dupont.com/content/dam/Dupont2.0/Products/water/literature/609-00378.pdf>. Access
682 date: 12 November 2018.

- 683 [39] Dow Chemical Company, FILMTEC Membranes Basics of RO and NF: Element Characteristics,
684 http://msdssearch.dow.com/PublishedLiteratureDOWCOM/dh_0071/0901b803800710df.pdf.
685 Access date: 12 November 2018.
- 686 [40] Dow Chemical Company, FILMTEC Membranes System Design: Introduction,
687 http://msdssearch.dow.com/PublishedLiteratureDOWCOM/dh_0043/0901b803800435bd.pdf?filepa
688 [th=liquidseps/pdfs/noreg/609-02046.pdf](http://msdssearch.dow.com/PublishedLiteratureDOWCOM/dh_0043/0901b803800435bd.pdf?filepath=liquidseps/pdfs/noreg/609-02046.pdf). Access date: 12 November 2018.
- 689 [41] Dow Chemical Company, FILMTEC XLE-2540 Membranes - Extra Low Energy Elements for
690 Commercial Systems,
691 <http://www.dupont.com/content/dam/Dupont2.0/Products/water/literature/609-00349.pdf>. Access
692 date: 12 November 2018.
- 693 [42] Dow Chemical Company, FILMTEC LE-4040 Membranes - Fiberglassed Elements for Light
694 Industrial Systems, <https://www.lenntech.com/Data-sheets/Dow-Filmtec-LE-4040.pdf>. Access date:
695 12 November 2018.
- 696 [43] B.S. Richards, G.L. Park, T. Pietzsch, A.I. Schäfer, Renewable energy powered membrane
697 technology: Safe operating window of a brackish water desalination system, *Journal of Membrane*
698 *Science*, 468 (2014) 400-409.
- 699 [44] A.I. Schäfer, J. Shen, B.S. Richards, Renewable energy powered membrane technology:
700 Removal of natural organic matter and fluoride in Tanzanian communities, *npj Nature Clean Water*,
701 24 (2018) 1-10.
- 702 [45] A.F. Derradji, S. Taha, G. Dorange, Application of the resistances in series model in
703 ultrafiltration, *Desalination*, 184 (2005) 377-384.
- 704 [46] G. Schock, A. Miquel, Mass transfer and pressure loss in spiral wound modules, *Desalination*,
705 64 (1987) 339-352.
- 706 [47] J. Mulder, *Basic Principles of Membrane Technology*, Springer, Netherlands, 1996.
- 707 [48] I.E. Idelchik, *Handbook of Hydraulic Resistance*, Begell House Publishers, USA, 2007.
- 708 [49] MathWorks, Hydraulic resistance in pipe bend,
709 <https://www.mathworks.com/help/phymod/hydro/ref/pipebend.html>. Access date: 12 November
710 2018.
- 711 [50] K. Boussu, Y. Zhang, J. Cocquyt, P. Van der Meeren, A. Volodin, C. Van Haesendonck, J.A.
712 Martens, B. Van der Bruggen, Characterization of polymeric nanofiltration membranes for systematic
713 analysis of membrane performance, *Journal of Membrane Science*, 278 (2006) 418-427.
- 714 [51] I. Owusu-Agyeman, A. Jeihanipour, T. Luxbacher, A.I. Schäfer, Implications of humic acid,
715 inorganic carbon and speciation on fluoride retention mechanisms in nanofiltration and reverse
716 osmosis, *Journal of Membrane Science*, 528 (2017) 82-94.
- 717 [52] H. Choi, K. Zhang, D.D. Dionysiou, D.B. Oerther, G.A. Sorial, Influence of cross-flow velocity
718 on membrane performance during filtration of biological suspension, *Journal of Membrane Science*,
719 248 (2005) 189-199.

- 720 [53] J.S. Vrouwenvelder, C. Picioreanu, J.C. Kruithof, M.C.M. van Loosdrecht, Biofouling in spiral
721 wound membrane systems: Three-dimensional CFD model based evaluation of experimental data,
722 Journal of Membrane Science, 346 (2010) 71-85.
- 723 [54] J. Luo, Y. Wan, Effects of pH and salt on nanofiltration - A critical review, Journal of Membrane
724 Science, 438 (2013) 18-28.
- 725 [55] S.M.J. Zaidi, F. Fadhillah, Z. Khan, A.F. Ismail, Salt and water transport in reverse osmosis thin
726 film composite seawater desalination membranes, Desalination, 368 (2015) 202-213.
- 727 [56] Y. Marcus, Thermodynamics of solvation of ions. Part 5.-Gibbs free energy of hydration at
728 298.15 K, Journal of the Chemical Society, Faraday Transactions, 87 (1991) 2995-2999.
- 729 [57] L.A. Richards, B.S. Richards, B. Corry, A.I. Schäfer, Experimental energy barriers to anions
730 transporting through nanofiltration membranes, Environmental Science & Technology, 47 (2013)
731 1968-1976.
- 732 [58] Seametrics, Resolving flowmeter instability problems, in, USA, 2009.
- 733 [59] G.H. Keulegan, K.H. Beij, Pressure Losses for Fluid Flow in Curved Pipes, US Government
734 Printing Office, USA, 1937.
- 735 [60] H.M. Laborde, K.B. França, H. Neff, A.M.N. Lima, Optimization strategy for a small-scale
736 reverse osmosis water desalination system based on solar energy, Desalination, 133 (2001) 1-12.
- 737 [61] C. Charcosset, A review of membrane processes and renewable energies for desalination,
738 Desalination, 245 (2009) 214-231.
- 739 [62] G.J. Kirmeyer, Guidance Manual for Monitoring Distribution System Water Quality, American
740 Water Works Association, USA, 2002.
- 741 [63] Dow Chemical Company, Dow Water and Process Solutions - Levels of Separation of IX, RO,
742 NF, UF, https://dowwater.custhelp.com/app/answers/detail/a_id/477. Access date: 12 November
743 2018.
744
745

746 **SUPPLEMENTARY INFORMATION**

747
748 **Renewable energy powered membrane technology: experimental**
749 **investigation of system performance with variable module size and fluctuating**
750 **energy**

751
752 *Junjie Shen^{1,2,3}, Azam Jeihanipour⁴, Bryce S. Richards^{2,4}, Andrea I. Schäfer^{3,5*}*

753
754 *¹ Centre for Advanced Separations Engineering, University of Bath, Bath BA2 7AY,*
755 *United Kingdom*

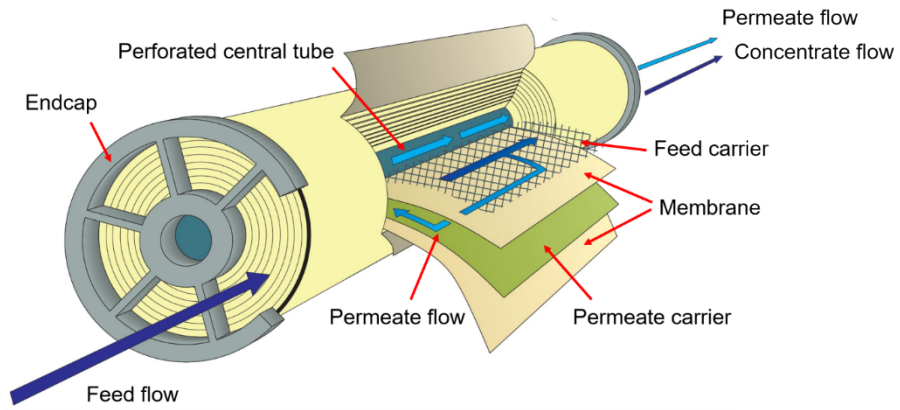
756 *² School of Engineering and Physical Sciences, Heriot-Watt University, Edinburgh*
757 *EH14 4AS, United Kingdom*

758 *³ Water and Environmental Science and Engineering, Nelson Mandela African Institute of*
759 *Science and Technology, Arusha, Tanzania*

760 *⁴ Institute of Microstructure Technology (IMT), KIT, Hermann-von-Helmholtz-Platz 1,*
761 *76344 Eggenstein-Leopoldshafen, Germany*

762 *⁵ Membrane Technology Department, Institute of Functional Interfaces (IFG-MT),*
763 *Karlsruhe Institute of Technology, Hermann-von-Helmholtz-Platz 1, 76344 Eggenstein-*
764 *Leopoldshafen, Germany*

779



780

781

782 Figure S1 Graphic of a spiral wound element

783

784

785

786

787

788

789

790

791

792

793

794

795

796

797

798

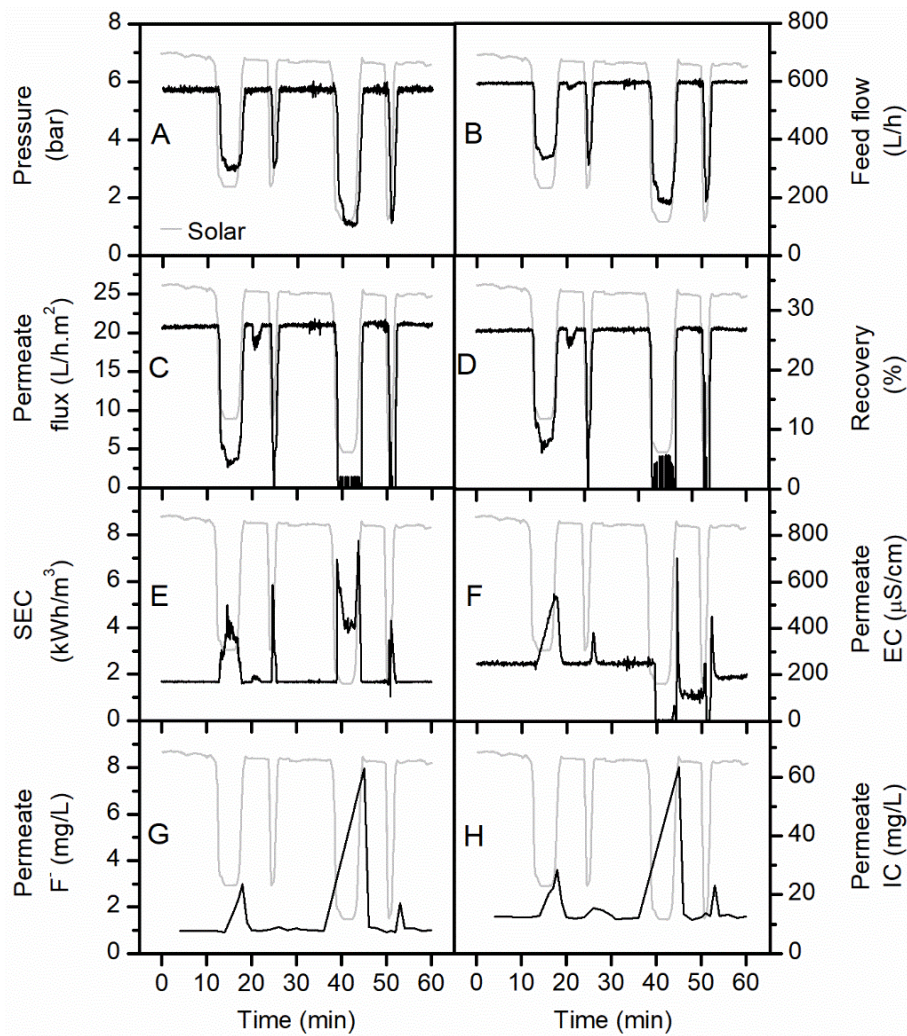
799

800

801

802

803



804

805

806

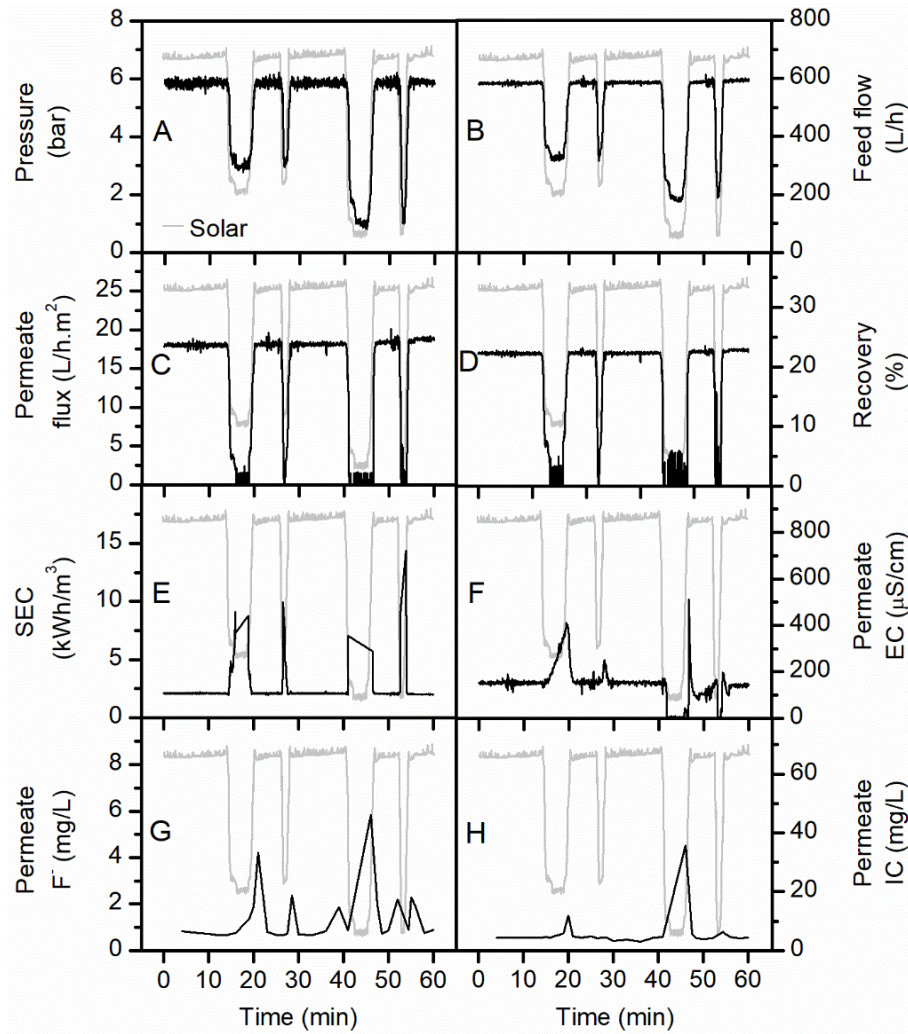
807

808

809

810

Figure S2 Instantaneous system performance of 1× 4" NF90 module over 60 min of the solar day: (A) pressure, (B) feed flow, (C) flux, (D) recovery, (E) SEC, (F) permeate EC, (G) permeate F⁻ concentration, (H) permeate IC concentration



812

813

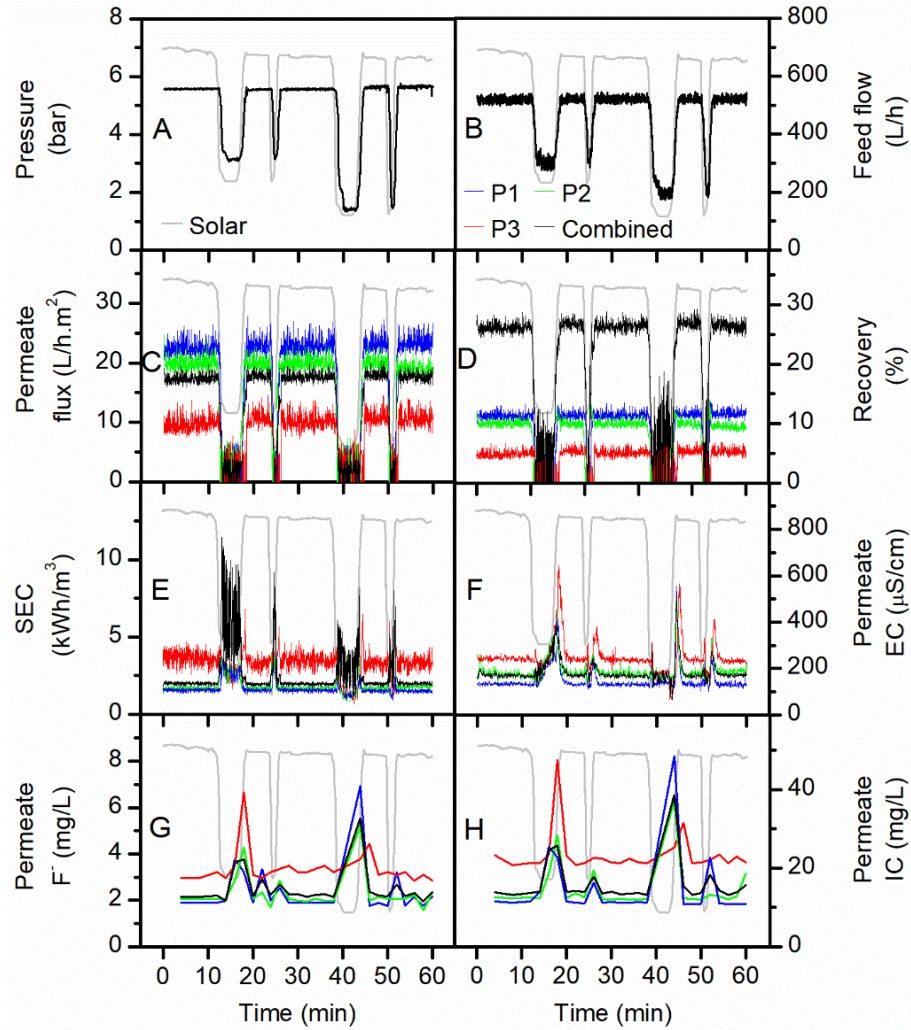
814

815

816

817

Figure S3 Instantaneous system performance of 1× 4" BW30LE module over 60 min of the solar day: (A) pressure, (B) feed flow, (C) flux, (D) recovery, (E) SEC, (F) permeate EC, (G) permeate F⁻ concentration, (H) permeate IC concentration



819

820

821

822

823

824

825

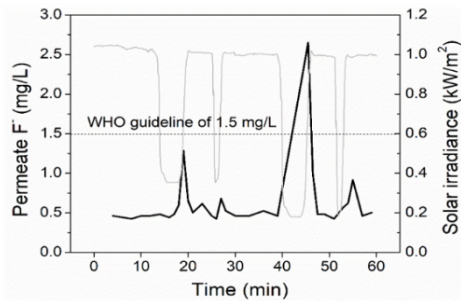
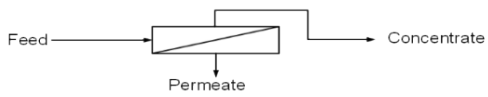
826

Figure S4 Instantaneous system performance of 3x2.5" XLE module over 60 min of the solar day: (A) pressure, (B) feed flow, (C) flux, (D) recovery, (E) SEC, (F) permeate EC, (G) permeate F⁻ concentration, (H) permeate IC concentration

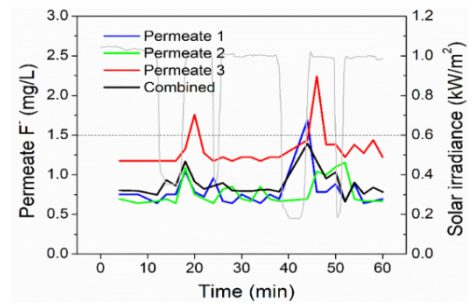
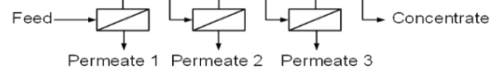
Highlights

- ◆ Tanzanian brackish water was treated by a photovoltaic powered NF/RO system
- ◆ Two configurations of NF/RO modules with the same membrane area were investigated during a fluctuation period
- ◆ The overall performance of the 1× 4" module was superior to the 3× 2.5" module
- ◆ The third element of the 3× 2.5" module reduced overall performance significantly
- ◆ The cumulative permeate fluoride of BW30, BW30LE and NF90 could meet the guideline

1 x 4" module



3 x 2.5" module



1 **Renewable energy powered membrane technology:**
2 **experimental investigation of system performance with**
3 **variable module size and fluctuating energy**

4
5 *Junjie Shen^{1,2,3}, Azam Jeihanipour⁴, Bryce S. Richards^{2,4}, Andrea I. Schäfer^{3,5*}*

6
7 ¹ *Centre for Advanced Separations Engineering, University of Bath, Bath BA2 7AY,*
8 *United Kingdom*

9 ² *School of Engineering and Physical Sciences, Heriot-Watt University, Edinburgh*
10 *EH14 4AS, United Kingdom*

11 ³ *Water and Environmental Science and Engineering, Nelson Mandela African Institute of Science*
12 *and Technology, Arusha, Tanzania*

13 ⁴ *Institute of Microstructure Technology (IMT), KIT, Hermann-von-Helmholtz-Platz 1, 76344*
14 *Eggenstein-Leopoldshafen, Germany*

15 ⁵ *Membrane Technology Department, Institute of Functional Interfaces (IFG-MT), Karlsruhe*
16 *Institute of Technology, Hermann-von-Helmholtz-Platz 1,*
17 *76344 Eggenstein-Leopoldshafen, Germany*

18
19
20 **Separation and Purification Technology**

21
22 Submitted **9 April 2018**

23 Resubmitted **12 November 2018 & 2 March 2019**

24
25
26
27
28
29
30
31
32 *corresponding author: Prof. Andrea I. Schäfer, +49 (0)721 608 26906,
33 Andrea.Iris.Schaefer@kit.edu

34 **Abstract**

35 Integration of renewable energy and membrane filtration technologies such as nanofiltration
36 (NF) and reverse osmosis (RO) can provide drinking water in places where freshwater is scarce and
37 grid electrical connections are unavailable. This study investigated a directly-connected photovoltaic-
38 powered membrane system under fluctuating solar conditions. Specifically, two configurations of
39 NF/RO membranes with the same membrane area were investigated: a) 1× 4" module, which
40 contained one 4" NF/RO element; and b) 3× 2.5" module, which contained three 2.5" NF/RO
41 elements in series. A high fluoride brackish water ($[F^-] = 56.2$ mg/L, total dissolved solids [TDS] =
42 4076 mg/L) collected from northern Tanzania was treated by different membranes in the two
43 configurations. Performance indicators such as flux, specific energy consumption, and permeate F^-
44 concentration were monitored over a 60-min period of energy fluctuation that are part of a typical
45 solar day. The results showed that the overall performance of the 1× 4" module was superior to that
46 of the 3× 2.5" module. This is because the performance of a 3× 2.5" module degraded significantly
47 from the first element to the third element due to the increased feed concentration and the decreased
48 net driving pressure. Three 1×4" modules (BW30, BW30LE and NF90) and one 3×2.5" module
49 (BW30) were able to meet the drinking water guideline for fluoride. During cloud periods, the
50 transient permeate F^- concentration exceeded the guideline value due to insufficient power, however
51 the cumulative permeate F^- concentration was always well below the guideline. The photovoltaic-
52 powered membrane system equipped with the above modules provides a promising solution for
53 addressing drinking water problems in remote and rural areas.

54

55

56 **Keywords:** brackish water; desalination; module size; fluoride; energy fluctuation; nanofiltration;
57 reverse osmosis

58

59

60

61 **1. Introduction**

62 The ever-increasing demand for fresh water and clean energy are among the major issues that
63 humans will face and need to solve in the 21st century [1]. The two issues are intertwined via the
64 energy-water nexus, meaning here that drinking water treatment and supply will always require
65 energy [2]. Extreme cases can be found in the many remote locations in both developed and
66 developing countries, which are far away from both centralized water and grid electricity supplies,
67 and where natural freshwater resources are scarce as well [3, 4]. In such cases, the integration of
68 renewable energy (RE) technologies with membrane filtration technologies, namely nanofiltration
69 (NF) and reverse osmosis (RO), provides a sustainable solution for this issue [3-5]. For example,
70 many photovoltaic (PV) powered membrane systems have been successfully implemented throughout
71 the world [6-10]. The figure-of-merit for system performance is typically the specific energy
72 consumption (SEC, units: kWh/m³), which represents how much electricity is required to produce
73 1 m³ of clean drinking water. The SEC is dependent on feed water salinity, system size, and
74 membrane type [3, 11].

75 In most PV-powered membrane systems, batteries are used to compensate for variations in
76 solar irradiance [6, 8, 12, 13]. Nevertheless, batteries exhibit several disadvantages such as reducing
77 the overall system efficiency, high capital and maintenance costs, and potential negative
78 environmental impacts in case of improper disposal [7, 14]. Therefore, it has been suggested to avoid
79 the use of batteries in such membrane systems to increase the efficiency and robustness, while
80 decreasing costs [9, 14-16]. However, in such batteryless systems the DC power produced by the PV
81 modules is directly coupled to the pump motor. The system is naturally subjected to widely varying
82 energy availability, which arises from the Earth's rotation, as well as landscape and weather
83 conditions, such as clouds, wind and ambient temperature [17]. The fluctuating current produced by
84 the PV modules subjects the NF/RO membranes integrated into such systems to fluctuations in
85 pressure and flow rate, which affects their flux and permeate water quality [9, 14, 18]. Additionally,
86 manufacturer of NF/RO membranes typically recommend to operate the membrane system in a
87 constant permeate flow rate to increase the life time of the membrane [19]. Richards *et al.* [18]
88 investigated the effects of fluctuating energy on retention of dissolved contaminants from real water
89 using a PV-powered NF/RO system. It was found that fluctuations in pressure and feed flow, as a
90 result of variation in solar irradiance, impacted the removal of solutes whose retention mechanism
91 was convection/diffusion. However, solutes that were retained via size exclusion and charge repulsion
92 were not affected by fluctuations in solar energy. It has been shown that when a batteryless PV-
93 powered NF/RO system was working under fluctuating conditions, even though the flux was often
94 low, a satisfactory quality of water at a low SEC could be delivered [17, 20]. Further, there is a

95 potential for the NF/RO membrane to possibly benefit from steps in the solar irradiance due to
96 disruption of the concentration polarization layer via a naturally induced backwash occurring when
97 the pump switched off [17].

98 Currently, spiral wound (SW) modules are the most widely used membrane modules for
99 NF/RO, thanks to their large membrane packing area, high design flexibility, and manufacturability
100 [21]. The construction of a typical SW module can be found in Figure S1. The basic component in a
101 SW module is membrane envelope, which is made of two flat-sheet membranes sealed on three edges,
102 with a permeate carrier filled in between [22, 23]. The achievable performance of a SW module
103 depends not only on the physicochemical characteristics of membrane active surface, but also on the
104 module size parameters, such as membrane envelope number and membrane dimensions [22, 24].
105 However, there has been little research conducted on the effect of module size on batteryless PV-
106 powered membrane systems. Knowledge of the performance of different module sizes under energy-
107 fluctuating conditions is needed for system planning and design, especially for remote and developing
108 areas. It should be noted that during operation with fluctuating energy feed flow and transmembrane
109 pressure vary. This means that pressure drop, concentration polarization (and with this the osmotic
110 pressure at the membrane surface) vary significantly more than in conventionally operated membrane
111 systems. Further, the availability of direct current (DC) equipment such as pumps that are suitable
112 for small systems remains limited. In a scenario where salinity is high, rejection is high and
113 permeability is good and the pressure that can be supplied by the pump is limited, the osmotic pressure
114 may exceed the applied pressure and water permeation is no longer possible. This is typically most
115 likely to happen at the outlet of the module, while during fluctuation this scenario may be more
116 common. In consequence, the design cannot always maintained ideal and studies are aimed at finding
117 the safe operating window (SOW) for a particular water. Remaining within this SOW is a matter of
118 a suitable control system.

119 This paper addresses this knowledge gap by utilizing two types of SW modules (with
120 comparable membrane areas) in treating a Tanzanian brackish water with high fluoride contents. In
121 Tanzania, excessive fluoride in drinking water has been recognized to cause large-scale health
122 problems, including dental and skeletal fluorosis [25-27]. Current defluoridation methods available
123 in Tanzania, such as adsorption and precipitation, are far from satisfactory due to insufficient removal
124 capacity and complicated maintenance [28-30]. Previous work from has demonstrated that NF/RO
125 membranes are effective in removing fluoride from natural waters in Tanzania [10, 20, 31]. In this
126 study, a batteryless PV-powered membrane system with two types of SW modules will be operated
127 under energy fluctuations. Variations of operating parameters (pressure, feed flow) and performance
128 indicators (flux, SEC, permeate concentration) of the two modules will be compared. In addition, the

129 performance degradation of each element within the 3× 2.5" module will be investigated. The
130 concentration polarization of such operation was calculated for three energy levels observed from the
131 experimental study using computational fluid dynamics (CFD) for this variable module configuration
132 to understand the transport phenomena [32].
133

134 **2. Materials and methods**

135 **2.1. Water characteristics**

136 A high fluoride content brackish water from a borehole in Mdori, a remote village near Lake
137 Manyara in northern Tanzania (GPS coordinates: S03°47.273', E035°51.138'), was used as natural
138 water to be treated by NF/RO. 5000 L of water was collected by a water truck on 17 January, 2014.
139 The pH and electrical conductivity (EC) were measured by a pH/conductivity meter (Multi 340i,
140 WTW, Germany). Turbidity was measured using a turbidity meter (TN100, Eutech, Netherlands).
141 Total organic carbon (TOC) and inorganic carbon (IC) were determined by a portable TOC analyzer
142 with autosampler (Sievers 900, GE Analytical Instruments, USA). Fluoride ion (F⁻) was determined
143 by an ion-selective electrode connected to a pH meter (826 pH Mobile Meter, Metrohm, UK).
144 Chloride (Cl⁻) and sulphate (SO₄²⁻) ions were analyzed by an ion chromatograph (IC 790, Metrohm,
145 Germany). Metal and non-metallic elements were measured via inductively coupled plasma optical
146 emission spectrometry (ICP-OES) (Vista-PRO CCD Simultaneous ICP-OES, Varian, Netherlands).
147 Methods of IC and ICP-OES were described by Shen et al. [20]. Total dissolved solid (TDS) was
148 calculated as the sum of major cations and anions.

149 The water quality components are presented in Table 1. The water was characterized by high
150 alkalinity (pH 9.7) and high salinity (TDS 4076 mg/L), according to the World Health Organization
151 (WHO) guideline for drinking water [33]. The dominant ions were Na⁺, SO₄²⁻, Cl⁻, and IC, including
152 CO₃²⁻ and HCO₃⁻. High levels of salinity and turbidity have no health significance, but they reduce
153 the acceptability of drinking water in terms of its taste, odor and appearance [33]. The F⁻ concentration
154 was 56.2 mg/L, which exceeded the WHO guideline of 1.5 mg/L by more than 37 times. Such high
155 level of F⁻ poses a genuine health risk of dental and skeletal fluorosis [25]. Therefore, F⁻, IC and EC
156 (represents salinity) were the three target components to treat in order to produce acceptable drinking
157 water from the Mdori brackish water.

158
159

160 Table 1 Water quality at Mdori borehole in northern Tanzania (GPS coordinates: S03°47.273',
 161 E035°51.138'), compared to WHO guidelines
 162

Parameter	Unit	Value	WHO guideline [33]
pH (25 °C)	–	9.7	6.5-8.5
EC (25 °C)	µS/cm	4940	–
TDS	mg/L	4076 ^a	1000 ^b
Turbidity	NTU	15.8	1 ^c
TOC	mg/L	5.3	–
IC	mg/L	430.0	–
F ⁻	mg/L	56.2	1.5
Cl ⁻	mg/L	268.0	250 ^b
SO ₄ ²⁻	mg/L	306.1	250 ^b
Al	mg/L	0.1	0.1 ^d
B	mg/L	1.9	2.4
Ca	mg/L	1.6	300 ^b
Fe	mg/L	0.2	0.3 ^b
K	mg/L	16.3	–
Mg	mg/L	0.5	–
Na	mg/L	1358.1	200 ^b
P	mg/L	0.7	–
Si	mg/L	17.3	–
Sr	mg/L	0.1	–

163 ^a Calculated as the sum of cations and anions, the charge difference between cations and anions < 5%.

164 ^b Based on average taste thresholds.

165 ^c Based on disinfection effectiveness.

166 ^d Based on optimization of the coagulation process.

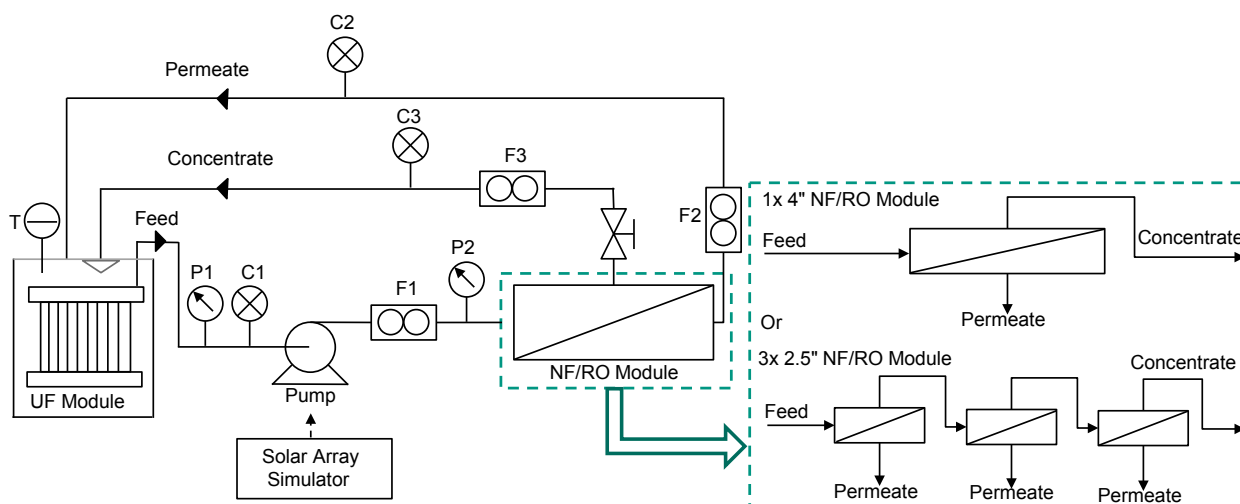
167 2.2. System design and membrane characteristics

168 An integrated PV-powered membrane system was used for the experiments. The filtration
 169 system combines ultrafiltration (UF) and NF/RO processes. The UF stage was used to remove
 170 particles, viruses and bacteria while the NF/RO stage was for desalination. A schematic is shown in
 171 Figure 1, while full details of the system have been published elsewhere [20, 34, 35]. As part of the
 172 design concept this system includes some unusual features; the system is operated at relatively low
 173 recovery (10-30%) and there is no energy recovery in the system (in form of a booster pump) that
 174 would enhance this recovery. The reason is firstly that very few suitable DC components exist to
 175 allow such operation for non-seawater systems. Secondly, provided the water is of such quality that

176 after the physical disinfection stage (UF) it can be safely used for washing or showering purposes,
 177 then this approach allows to avoid concentrate production. This is highly beneficial in remote areas
 178 where no adequate treatment of such concentrates is feasible. In this case this is indeed possible, as
 179 the feed water was used for laundry where fluoride is not a concern and the marginal increase in
 180 salinity can be tolerated.

181 The NF/RO elements were spiral wound in 40" (1 m) length and in two different diameters,
 182 2.5" and 4". Two different configurations, or modules, of the NF/RO elements were tested. The first
 183 module contained one 4" NF/RO element (denoted as the 1× 4" module), and the second module
 184 contained three 2.5" elements in series (denoted as the 3× 2.5" module) such that the concentrate of
 185 the first element became the feed to the second, and the concentrate of the second the feed of the
 186 third. Therefore, the length of the 3× 2.5" module was triple the length of the 1× 4" module, while
 187 the cross-sectional area of the 3× 2.5" module was approximately one-third of that of the 1× 4"
 188 module. In the 1× 4" module, the permeate and concentrate streams were recirculated into the feed
 189 tank; in the 3× 2.5" module, the three permeate streams (one from each element) and the concentrate
 190 stream of the last element were recirculated to the feed tank, separately. Pressure, temperature, flow
 191 rate and EC sensors were installed on the feed, permeate and concentrate streams. The sensor details
 192 can be found in a previous publication [35]. As the system was adapted to install the 3× 2.5" module
 193 in the existing system, no additional pressure sensors were added and hence the pressure drop across
 194 the individual modules is not available. This was exacerbated by the concentrate pressure sensor being
 195 not fully functional. These are a design and operational shortfalls that could not be remedied during
 196 the field work. Data from the sensors were recorded by a datalogger at 2 second intervals and
 197 transferred to a laptop using LabVIEW 8.0 software.

198



199

200

201 Figure 1 Schematic of the PV-powered membrane system configurations equipped with either 1× 4"
202 module or 3× 2.5" NF/RO module. Sensors are marked as T (temperature), P (pressure transducer),
203 C (EC) and F (flow).

204

205 Five types of NF/RO membrane, namely NF270, BW30, NF90, BW30LE and XLE (all
206 sourced from DOW Chemical, USA) were used. NF270 and NF90 are NF membranes while BW30,
207 BW30LE and XLE are brackish water RO membranes. Membrane specifications provided by the
208 manufacturer are summarized in Table 2. It is assumed that the membrane envelopes in both 2.5" and
209 4" elements have the same dimensions. The difference in their diameters are only due to different
210 numbers of envelopes that are wound into the 2.5" and 4" elements.

211

212 Table 2 Membrane specifications as provided by the manufacturer [36-42]

Type	Active area (m ²)	Permeance ^a (L/m ² .h.bar)	Retention (%)	Maximum feed flow (L/h)	Maximum pressure (bar)	Maximum recovery (%)
4" BW30	7.2	3.4	99.5 ^b	3600	41	90
2.5" BW30	2.6	3.3	99.5 ^b	1400	41	90
4" NF270	7.6	10.8	>97.0 ^c	3600	41	90
2.5" NF270	2.6	10.7	>97.0 ^c	1400	41	90
4" NF90	7.6	8.7	>97.0 ^c	3600	41	90
4" BW30LE	7.6	4.6	99.0 ^d	3600	41	90
2.5" XLE	2.6	7.4	99.0 ^e	1400	41	90

213 ^a Permeance (P) was calculate using the equation $P = \frac{Q_P}{A \times p}$, where Q_P was permeate flow at provided test conditions, p
214 is applied pressure and A is membrane active area.

215 ^b Test condition: 2000 mg/L NaCl at 15.5 bar, 15% recovery, 25 °C

216 ^c Test condition: 2000 mg/L MgSO₄ at 4.8 bar, 15% recovery, 25 °C

217 ^d Test condition: 2000 mg/L NaCl at 10.3 bar, 15% recovery, 25 °C

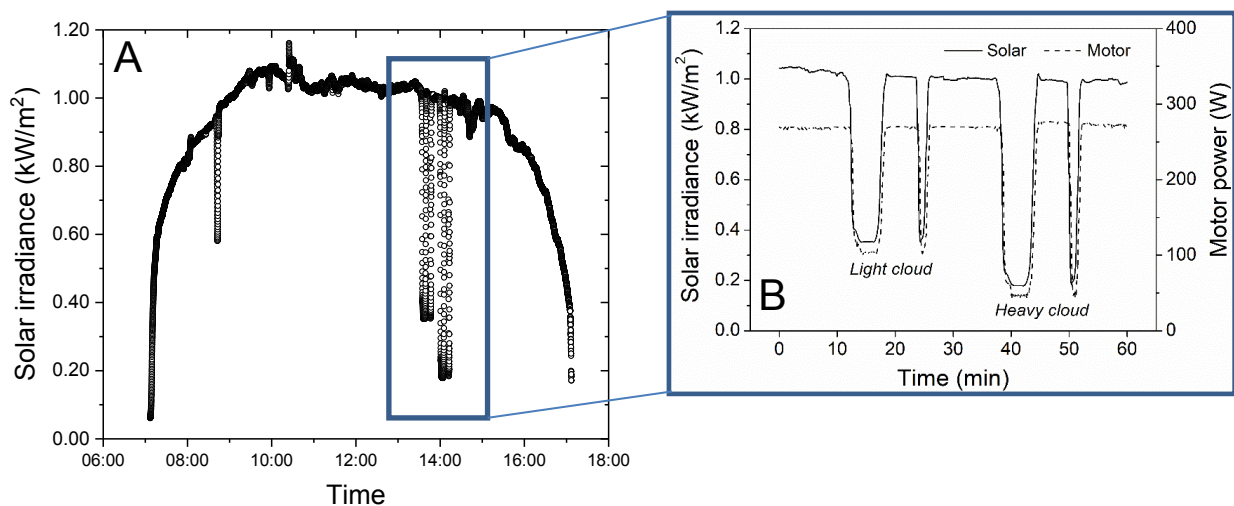
218 ^e Test condition: 500 mg/L NaCl at 6.9 bar, 15% recovery, 25 °C.

219

220 2.3. Experimental procedure

221 In order to have identical solar power quality for all experiments, a solar array simulator (SAS,
222 E4350B, Agilent Technologies, US) was used to power the helical rotor pump (Mono Sun-Sub,
223 Australia). When supplied with solar irradiance data, the SAS functions as a DC power supply that is
224 able to simulate the output of PV modules, thus enabling variable but repeatable solar conditions to
225 be investigated. The simulated PV modules are the ones actually mounted on the PV-membrane

226 system (BP Solar BP3150S, each provide a maximum power of 150 W). A 60-min period of solar
 227 irradiance data were recorded in a sunny day during the dry season in Tanzania. The solar irradiance
 228 and the resulting motor power of the pump are shown in Figure 2 in the context of the full day of
 229 solar irradiance (Figure 2A). The solar irradiance data in Figure 2B are characterized by three features:
 230 (i) the maximum intensity of about 1 kW/m², which occurs under cloudless skies; (ii) two short peaks
 231 of about 2 min duration occurring at $t = 24$ and $t = 50$ min with a minimum solar intensity of 0.36 and
 232 0.19 kW/m², respectively; and (iii) two longer duration peaks (6 to 7 min) at $t = 15$ and $t = 40$ with a
 233 minimum solar irradiance of 0.35 and 0.18 kW/m², respectively. These dips in solar irradiance occur
 234 due to passing clouds. From now on, peaks with 0.35 – 0.36 kW/m² intensity will be referred to as
 235 ‘light cloud period’ and peaks with 0.18 – 0.19 kW/m² intensity as ‘heavy cloud period’, as indicated
 236 in Figure 2. During the period of maximum intensity of solar irradiance (1 kW/m²) the power
 237 consumed by the pump was relatively constant at 270 W, which resulted in a constant pressure and
 238 feed flow in all experiments.
 239



240 Figure 2 Solar irradiance and the resulting motor power during (A) the full solar day with a controlled
 241 fluctuation and (B) the 60-min test period used for the experiments with different membranes and
 242 configurations

243
 244 As there was only one set of sensors in the permeate stream, it was impossible to
 245 simultaneously monitor the permeate stream of every element in the 3×2.5" module. Therefore, three
 246 repetitive experiments were conducted and in each experiment, one of the three permeate streams was
 247 connected to the sensors. Water samples from each permeate stream were manually collected every
 248 two minutes for further analyses. Prior to each experiment, the back-pressure valve was adjusted to a
 249 point where a similar feed flow was achieved at roughly the same pressure with different modules.
 250 The concept of such a “set-point” to enable fair comparison between different system configurations

251 was discussed in more detail in a previous paper [43]. The set-point for the different modules was
 252 chosen to be a pressure of 5.5 – 6.0 bar with a relatively low feed flow of 550 – 600 L/h. The following
 253 formulae were used to calculate the parameters to evaluate the performance of the system.

254

$$255 \quad R = \left(1 - \frac{C_P}{C_F}\right) \times 100\% \quad (1)$$

256

$$257 \quad Y = \left(\frac{Q_P}{Q_F}\right) \times 100\% \quad (2)$$

258

$$259 \quad \begin{aligned} J \\ = \frac{Q_P}{A} \end{aligned}$$

260 (3)

$$261 \quad SEC = \frac{I \times U}{Q_P} \quad (4)$$

262

$$263 \quad \begin{aligned} C_{3 \times 2.5} \\ = \frac{Q_{P1}C_{P1} + Q_{P2}C_{P2} + Q_{P3}C_{P3}}{Q_{P1} + Q_{P2} + Q_{P3}} \end{aligned} \quad (5)$$

264

$$265 \quad V_{cumulative} = \sum_{i=1}^t \left(\frac{Q_{Pi}}{1800}\right) \quad (6)$$

266

$$267 \quad \begin{aligned} C_{cumulative} \\ = \frac{\sum_{j=1}^t (C_{Pj} \times V_j)}{V_{cumulative}} \end{aligned} \quad (7)$$

268

269 In the above equations, C_F and C_P are the initial feed and permeate concentration (mg/L),
 270 respectively, Q_F and Q_P are the feed and permeate flow (L/h), respectively, R is retention (%), Y is
 271 recovery (%), J is flux (L/m².h), A is membrane active area (m²), SEC is specific energy consumption
 272 (kWh/m³), I is pump current (A), U is pump voltage (V), $C_{3 \times 2.5}$ is the fictitious permeate

273 concentration if three permeate streams of the $3 \times 2.5''$ module were merged (P1, P2, P3 refer to the
274 first, second and third permeate stream, repectively), $V_{cumulative}$ is the cumulative sum of permeate
275 water volume over time (L), $C_{cumulative}$ is the cumulative sum of permeate concentration over time
276 (mg/L). For each of the 2.5'' elements, the SEC was calculated using 1/3 of the motor power. To
277 calculate retention for the 2.5'' elements, the original feed concentration, fed to the first element, was
278 considered as feed concentration for all three elements in the $3 \times 2.5''$ module. Pressure drop, expected
279 in the order of 0.03 to 0.15 bar per m (or in this case per element), was not monitored. This pressure
280 drop will be higher for the $3 \times 2.5''$ module due to i) a smaller cross-sectional area and hence higher
281 crossflow velocity, and ii) three modules in series.

282

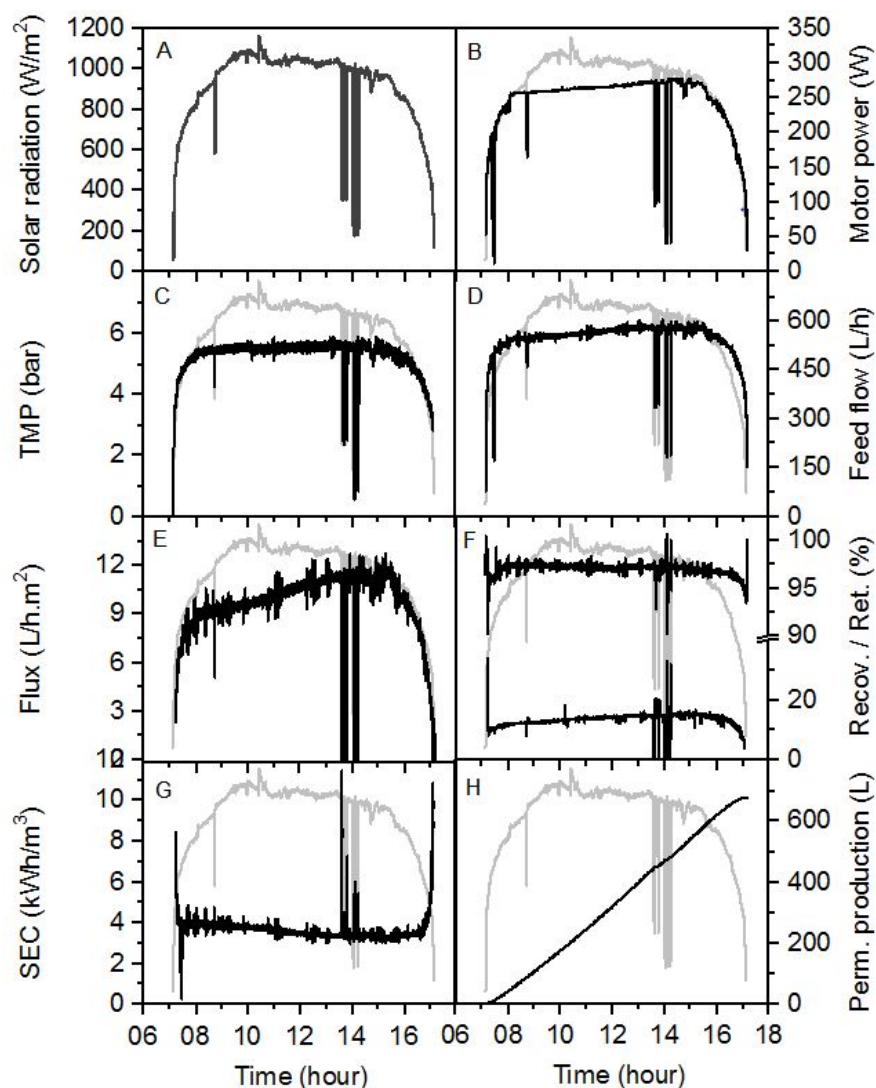
283 **3. Results & Discussion**

284 **3.1. Typical system performance over a solar day**

285 To set the work of different module configurations over the 60 min fluctuations period, a
286 typical result over a full day is shown in Figure 3 for the Mdori water and a 1× 4'' BW30 module. As
287 the sun rises in the morning (Figure 3A) the motor power (Figure 3B) is determined by the maximum
288 power point tracker and will drive the pump to provide the transmembrane pressure (TMP) (Figure
289 3C) and feed flow (Figure 3D). This results in a flux (Figure 3E) at a variable recovery and EC
290 retention (Figure 3F). Specific energy consumption (Figure 3G) can be calculated and ultimately the
291 amount of clean water (permeate) produced over such a solar day be determined (Figure 3F). Such
292 data was published previously with very detailed analysis for different waters [10] and for the same
293 water during field work [44] with a focus on transport mechanisms. The retention (in this graph that
294 of EC) varies with fluctuation because diffusion will play a significant role when the applied pressure
295 reduces. The same phenomena is typically observed for EC, IC and F.

296 Naturally the specific performance will change with membrane type, the main differences will
297 take place during the fluctuation where diffusion contributes disproportionately to permeate quality,
298 while during the maximum solar irradiation the performance of the membrane type can be deducted.
299 For this reason the further investigations are limited to this one hour fluctuation, taking very frequent
300 data readings. This results in a cumulative permeate volume of about 1/10th of a full solar day.

301



302

303 Figure 3 Typical full day experiment with Mdori water and 1×4'' module (BW30) with (A) Solar
 304 irradiance, (B) motor power, (C) transmembrane pressure (TMP), (D) feed flow, (E) flux, (F)
 305 recovery (*bottom*) and retention of electrical conductivity (*top*), (G) specific energy consumption
 306 (SEC), and (H) cumulative permeate production.

307 3.2. Performance of the 1×4'' and 3×2.5'' modules during cloudless periods

308 System performance under steady-state conditions was firstly studied as a point of reference
 309 for evaluating performance under fluctuating energy. The steady-state region was chosen to be
 310 between 34 and 36 min (Figure 2B). The results of NF270 and BW30 membranes in two module
 311 sizes (1×4'' and 3×2.5'') are presented in Table 3 and Table 4, respectively. The results of NF90,
 312 BW30LE and XLE membranes are presented in the Supplementary Information as Figure S2, S3, and
 313 S4, respectively.

314 Different modules of the same membrane obtained similar pressure and feed flow, confirming
 315 that the 'set-point' approach indeed provides a good basis for performance comparison. As shown in

316 Table 3, the 1× 4" module of NF270 produced permeate at a flux of 35.1 L/m².h and a recovery of
317 43.9%. The 3× 2.5" module of NF270 had a similar flux of 33.5 L/m² and a recovery of 49.3%. The
318 slightly larger difference in their recoveries was related to their different feed flows. The combined
319 SEC of the 3× 2.5" module was 0.98 kWh/m³, which was identical with that of the 1× 4" module.
320 When it comes to the individual elements, the flux and recovery decreased sharply from the first to
321 the third element. The flux decline was in general caused by a decreased net driving pressure and an
322 increased hydraulic resistance [45, 46]. The decrease of the net driving pressure was the result of (1)
323 the axial pressure drop along the feed channel, and (2) an increase in solute concentration and hence
324 in osmotic pressure due to water permeation and retention [23, 47]. The increased resistance included
325 (1) the friction resistance due to the prolonged flow path and (2) the local resistance when the
326 direction of flow was sharply changed (such as in endcaps and pipe bends) [23, 48, 49]. The SEC
327 increased from the first element to the third element accordingly.

328 Further, permeate EC, F⁻ and IC concentrations from the 3× 2.5" and 1× 4" modules of NF270
329 were compared (see Table 3). NF270 is known as a 'loose' NF membrane with a molecular weight
330 cut-off (MWCO) of 155 – 180 Da [31, 50]. NF270 rejects ions mainly based on charge repulsion [31,
331 51]. The permeate EC and IC of the 3× 2.5" module were both lower than that of the 1× 4" module.
332 This can be explained by the reduced concentration polarization in the 3× 2.5" module. Given that
333 the cross-sectional area of the 3× 2.5" module was only one-third of that of the 1× 4" module, the
334 crossflow velocity of the 3× 2.5" module was approximately triple that of the 1× 4" module at the
335 same feed flow. Therefore, the concentration polarization in the 3× 2.5" module was more reduced
336 by the higher crossflow velocity [52, 53]. A follow-up study using computational fluid dynamics has
337 revealed that the 3× 2.5" module had a lower wall concentration and a smaller boundary layer
338 thickness compared to the 1× 4" module [32]. Notably, the permeate F⁻ concentration of the 3× 2.5"
339 module was higher than those of the 1× 4" module. The negative effect of salinity and IC speciation
340 on F⁻ retention was attributed to charge screening and Donnan effect [51, 54, 55]. The permeate F⁻
341 concentrations of the 3× 2.5" and 1× 4" modules were both far beyond the WHO guideline of 1.5
342 mg/L and this membrane was clearly not suitable to produce potable water.

343 Within the 3× 2.5" module, the permeate concentrations increased sharply from the first
344 element to the third element. The permeate IC and F⁻ from the third element were approximately
345 doubled as compared with those from the first element. Such rapid degradation of permeate quality
346 was attributed to: (1) the increased feed concentration from first to third element; and (2) the
347 decreased net driving pressure due to the axial pressure drop and the increased osmotic pressure.

348

349 Table 3 Summary of performance indicators of the 1× 4" and 3× 2.5" modules of NF270 under steady-
 350 state operation during cloudless periods (1 kW/m² solar irradiance).

	1× 4 "module	3× 2.5 "module			
		Combined	First element	Second element	Third element
Flux (L/m ² .h)	35.1	33.5	42.2	30.7	27.7
Recovery (%)	43.9	49.3	20.7	15.0	13.6
SEC (kWh/m ³)	0.98	0.98	0.82	1.12	1.25
Permeate EC (μS/cm)	2012.3	1881.5	1554.6	1779.6	2492.3
Permeate F ⁻ (mg/L)	25.9	30.2	20.6	30.5	44.4
Permeate IC (mg/L)	176	154	107	154	227

351
 352 Not surprisingly, when comparing the performance of BW30 to NF270, the former exhibited
 353 a noticeably lower flux and higher SEC, but produced permeate with a higher quality (Table 4). The
 354 flux of the 1× 4" module of BW30 was 11.7 L/m².h, while the combined permeate flux of the 3× 2.5"
 355 module was 8.2 L/m².h. The lower flux of the 3× 2.5" module was because of a higher axial pressure
 356 drop (a lower net driving pressure) and a higher hydraulic resistance along the feed channel. This is
 357 due to the 3× 2.5" module being three times as long as the 1× 4" module as well as the higher velocity,
 358 even though the higher velocity is expected to reduce concentration polarization. Furthermore, the
 359 difference in flux between two modules was more significant for BW30 over NF270 due to a higher
 360 rejection and hence higher osmotic pressure difference resulting in a lower net driving pressure.
 361 Therefore the axial pressure drop probably had a bigger impact on BW30 than on NF270. The SEC
 362 of the 3× 2.5" module (4.24 kWh/m³) was higher than that of the 1× 4" module (3.21 kWh/m³) as a
 363 result of the lower flux. As a 'tight' RO membrane (MWCO 98 Da [50]), BW30 rejects ions primarily
 364 based on size exclusion [31]. The permeate EC of the 3× 2.5" module was lower than that of the 1×
 365 4" module, which suggests that the 3× 2.5" module was better than the 1× 4" module in rejecting total
 366 dissolved salts. However, the permeate F⁻ and IC concentrations of the 3× 2.5" module were slightly
 367 higher than those of the 1× 4" module. A possible explanation is that F⁻ and IC (*i.e.* CO₃²⁻ and HCO₃⁻)
 368 in the 3× 2.5" module were less retained than other larger anions that contributed to EC (such as Cl⁻
 369 and SO₄²⁻) by size exclusion [56, 57]. Noticeably, both modules managed to reduce the permeate F⁻
 370 concentration to meet the WHO guideline of 1.5 mg/L, even for the third element of the 3× 2.5"
 371 module.

372

373 Table 4 Summary of performance indicators of the 1× 4" and 3× 2.5" modules of BW30 under steady-
 374 state operation during cloudless periods (1 kW/m² solar irradiance).

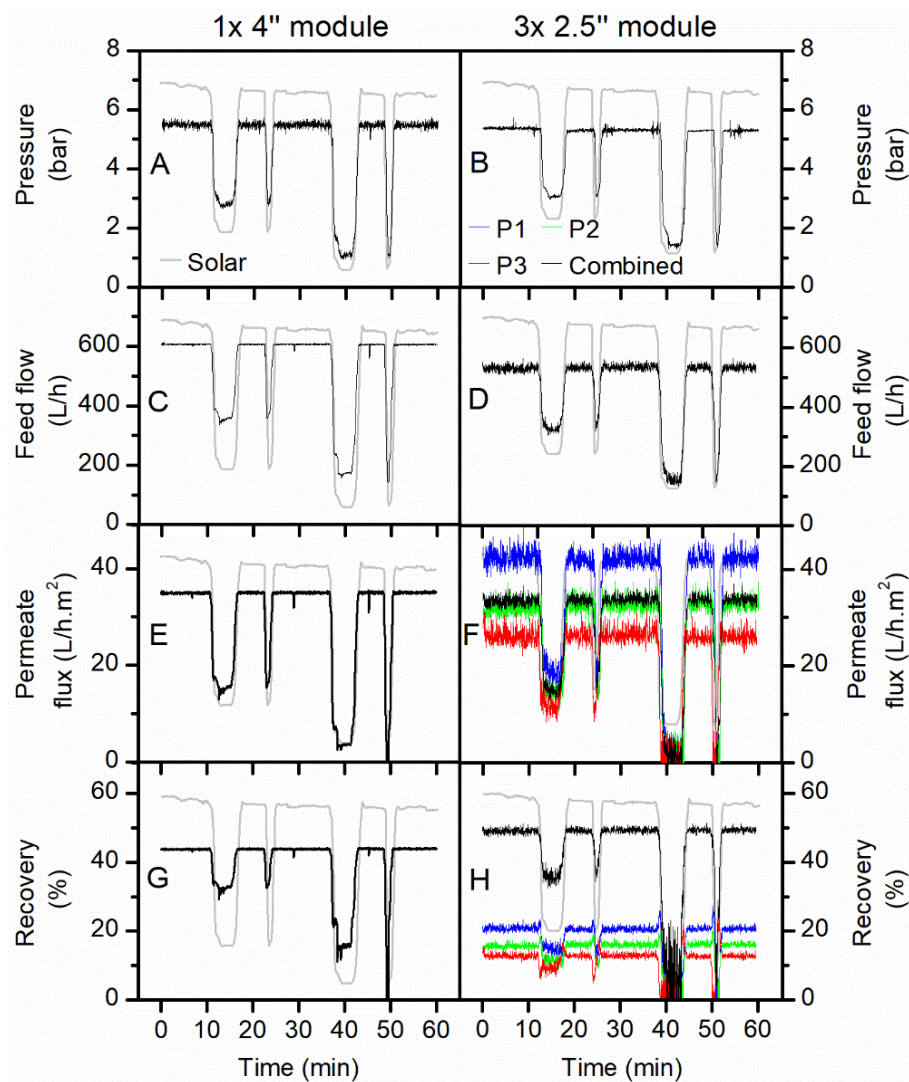
	1× 4 "module	3× 2.5 "module			
		Combined	First element	Second element	Third element
Flux (L/m ² .h)	11.7	8.2	10.9	9.4	4.2
Recovery (%)	14.4	11.4	5.1	4.4	1.9
SEC (kWh/m ³)	3.21	4.24	3.17	3.68	8.28
Permeate EC (μS/cm)	134.6	57.5	34.6	63.7	103.5
Permeate F ⁻ (mg/L)	0.5	0.8	0.6	0.8	1.2
Permeate IC (mg/L)	3.1	5.4	4.1	5.5	8.5

375

376 **3.3. Performance of the 1× 4" and 3× 2.5" modules of NF270 during cloudy periods**

377 The instantaneous performance of the 1× 4" and 3× 2.5" modules of the loose NF membrane
 378 NF270 are presented in Figure 4 and Figure 5, respectively. During the light and heavy cloud periods,
 379 the pressure and feed flow decreased sharply due to significant reduction in input power. For the 1×
 380 4" module, when the solar irradiance dropped from 1 to 0.2 kW/m² at 50 min, the pressure reduced
 381 from 5.5 to 0.9 bar and the feed flow reduced from 600 to 130 L/h (refer Figure 4A, C). The flux
 382 therefore decreased from 35 L/m².h to 0 L/m².h due to insufficient power (see Figure 4E), while the
 383 recovery dropped from 44% to 0% accordingly (see Figure 4G). As for the 3× 2.5" module, the
 384 variations of pressure and feed flow were very similar to those of the 1× 4" module, except that the
 385 feed flow was slightly lower (about 10%) than that of the 1× 4" module (see Figure 4B and D). The
 386 lower feed flow of the 3× 2.5" module was probably due to the increased hydraulic resistance. The
 387 fluxes – not only the flux from individual element but also the combined flux calculated from total
 388 permeate volume and total membrane area – dropped sharply during the light and heavy cloud periods
 389 and decreased to 0 L/m².h at 42 and 50 min (Figure 4F). The combined flux of the 3× 2.5" module
 390 was equal to the flux of the 1× 4" module. The recovery varied with the feed flow and permeate flux
 391 (Figure 4H). The combined recovery of the 3× 2.5" module, which equals to the sum of individual
 392 recoveries of each element, was slightly higher than the 1× 4" module because of its lower feed flow.

393



394

395 Figure 4 Comparison of the 1× 4" and 3× 2.5" modules of NF270 over 60 min of the solar day: (A,
 396 B) pressure, (C, D) feed flow, (E, F) flux, (G, H) recovery.

397

398 Notably, unstable readings were observed in feed flow and flux of the 3× 2.5" module. In
 399 order to maximize the use of space in the PV-powered membrane system, the three elements in series
 400 were arranged vertically from top to bottom. Consequently, the pipes connecting adjacent elements
 401 were sharply curved, which caused flow disturbances and thus affected flow measurement [58, 59].
 402 In addition, the tripled length of the flow path, the nearly tripled crossflow velocity, and the excessive
 403 number of endcaps in the 3× 2.5" module could also contribute to the unstable flow readings.
 404 Nevertheless, such unstable readings could be tolerated since they did not shield the measurement
 405 under fluctuating solar conditions, which was the specific focus of this study.

406 The results of the SEC and permeate quality produced by the two modules of NF270 are
 407 presented in Figure 5. The SEC mainly depends on the salinity of the water, the permeability of the
 408 membrane, the configuration of the system, the recovery, and the efficiency of the pump [60, 61].

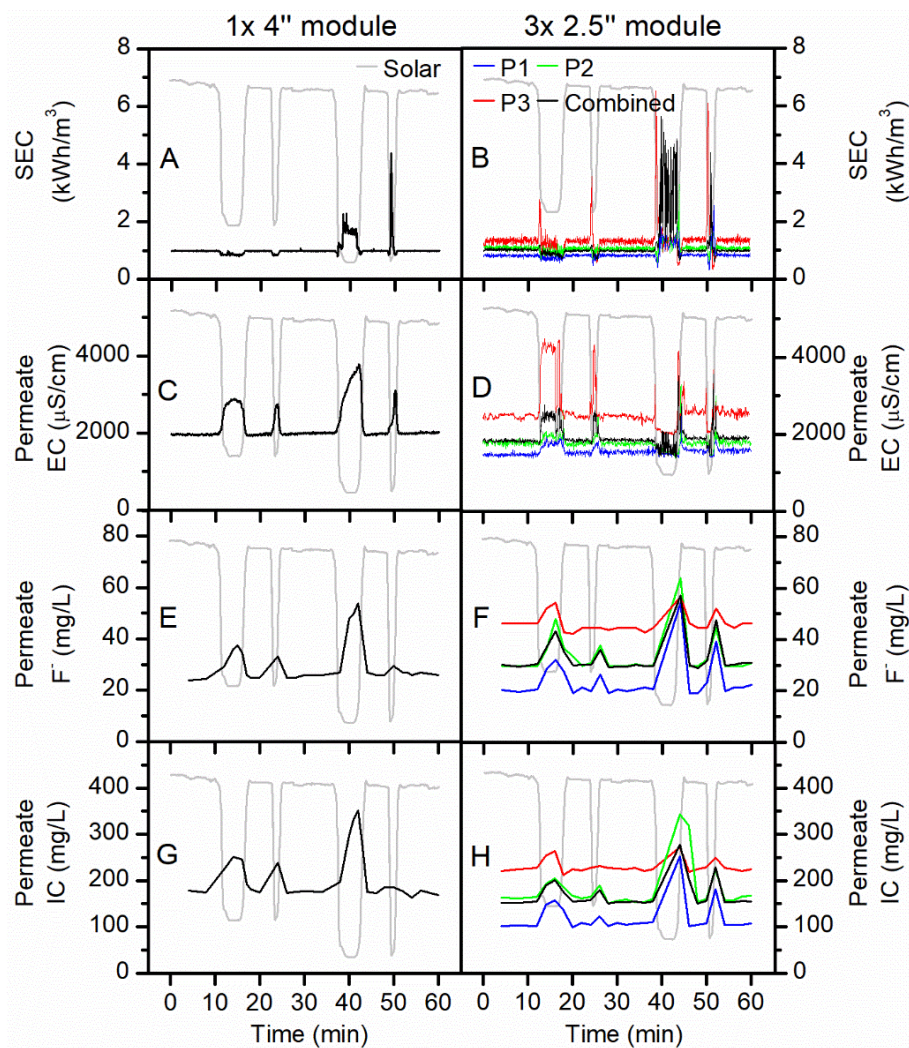
409 There was no markedly difference between the combined SEC of the 3× 2.5" module and the SEC of
410 the 1× 4" module under maximum intensity of solar irradiance. However, the SEC of the 3× 2.5"
411 modules demonstrated more dramatic volatility during the heavy cloud periods, which were attributed
412 to greater variations in the flux values (Figure 5B).

413 The 1× 4" module showed an increase in EC from 2000 to 3000 $\mu\text{S}/\text{cm}$ during the light cloud
414 period and from 2000 to 4000 $\mu\text{S}/\text{cm}$ during the heavy cloud period (Figure 5C). The increased salt
415 concentration during cloudy periods was primarily attributed to the severe drop in flux resulting in
416 less 'dilution'. Besides, the decline in feed flow reduced the crossflow velocity and thus probably
417 facilitated salt diffusion across the membrane [10]. In the 3× 2.5" module, the effect of energy
418 fluctuation on permeate EC was drastic for the third element while the effect was rather moderate for
419 the first two elements. As the available solar irradiance decreased from 1000 to 350 W/m^2 , during the
420 light cloud period, the permeate EC of the first element increased slightly from 1400 to 1800 $\mu\text{S}/\text{cm}$,
421 while the third element experienced a drastic increase from 2500 to 4500 $\mu\text{S}/\text{cm}$ (Figure 5D). During
422 the heavy cloud period, the flux reached 0 $\text{L}/\text{m}^2\cdot\text{h}$. The peak appearing at the end of the heavy cloud
423 period was due to the washing away of permeate that remained in the system during this downtime.

424 The permeate F^- and IC of both modules varied with solar irradiance in an analogous manner,
425 which exhibited an abrupt peak during the heavy cloud period (Figure 5E–H). This was again because
426 of the severe flux reduction. It is worthwhile mentioning that the permeate F^- and IC of the third
427 element of the 3× 2.5" module appears to be less affected by energy fluctuation, which seems
428 inconsistent with the trend of the permeate EC. This is in fact due to the two different measurement
429 methods of EC and F^-/IC , namely in-line monitoring and manual water sampling [62]. The permeate
430 EC was measured continuously by the in-line EC sensor, thereby the EC peaks were precisely
431 recorded. The permeate F^- and IC concentration, on the other hand, were measured intermittently
432 from discrete samples (samples were taken every two minutes). Inevitably there was some
433 unavoidable error in the peak positions and amplitudes.

434 Considering the flux, SEC and permeate quality, the performance of the first element of the
435 3× 2.5" module was better than the 1× 4" module. However, the deficient performance of the third
436 element of the 3× 2.5" module resulted in obtaining a similar overall performance compared to the
437 1× 4" module.

438



439

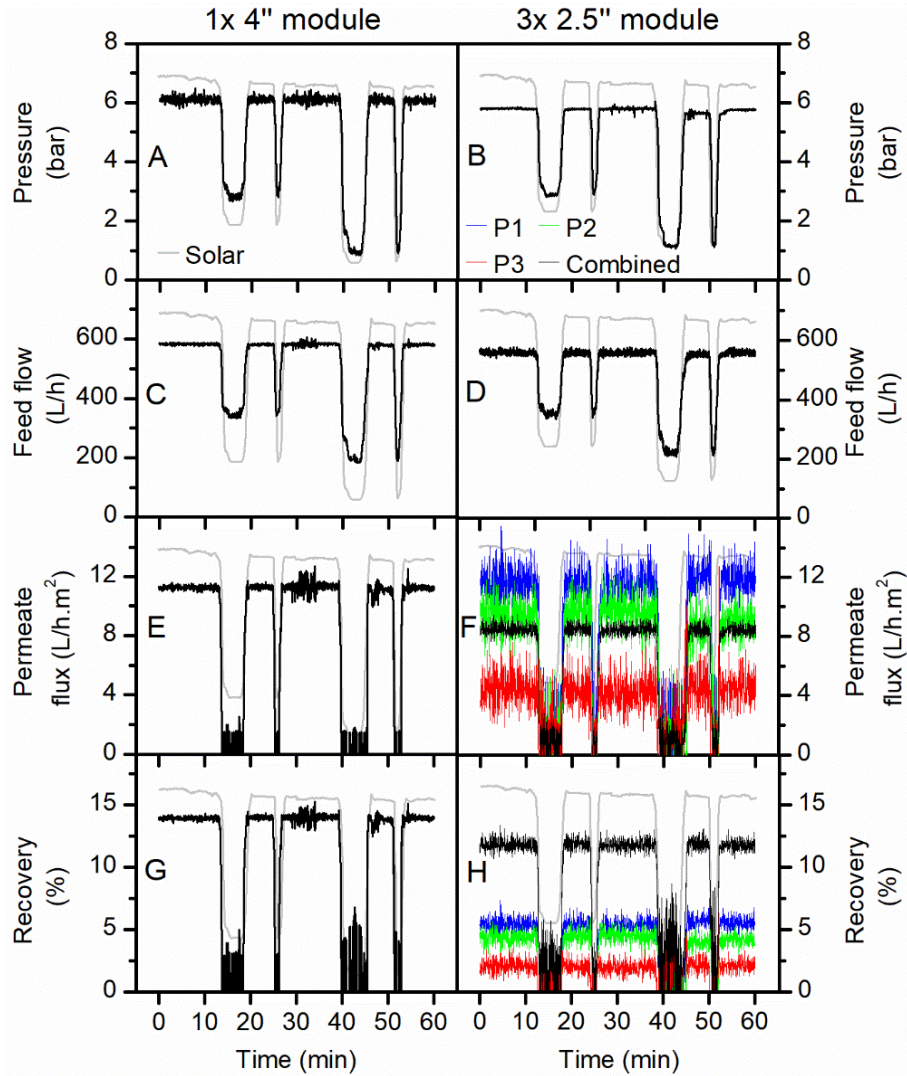
440 Figure 5 Comparison of the 1× 4" and 3× 2.5" modules of NF270 over 60 min of the solar day: (A,
 441 B) SEC, (C, D) permeate EC, (E, F) permeate F⁻ concentration, (G, H) permeate IC concentration.

442

443 3.4. Performance of the 1× 4" and 3× 2.5" modules of BW30 during cloudy periods

444 The effect of changing to a denser SW membrane with high salt retention, BW30, on the
 445 performance of the batteryless PV-powered system was studied as well. The results of the
 446 performance testing of the two configurations, 1× 4" and 3× 2.5" BW30 modules, are presented in
 447 Figure 6 and Figure 7. The pressure applied to both BW30 module types were nearly identical, as
 448 were the feed flows (Figure 6A–D). The unstable readings in feed flow and flux of the 3× 2.5" module
 449 under steady-state conditions were attributed to flow disturbances, as explained earlier for NF270.
 450 Flux and recovery of the 1× 4" module of BW30 was notably better than the 3× 2.5" module (Figure
 451 6E–H), which was attributed to a lower axial pressure drop and a lower hydraulic resistance. In
 452 consequence, the combined SEC of the 3× 2.5" module was higher than that of the 1× 4" module, let
 453 alone the extremely high SEC of the third element of the 3× 2.5" module (Figure 7A,B). As discussed

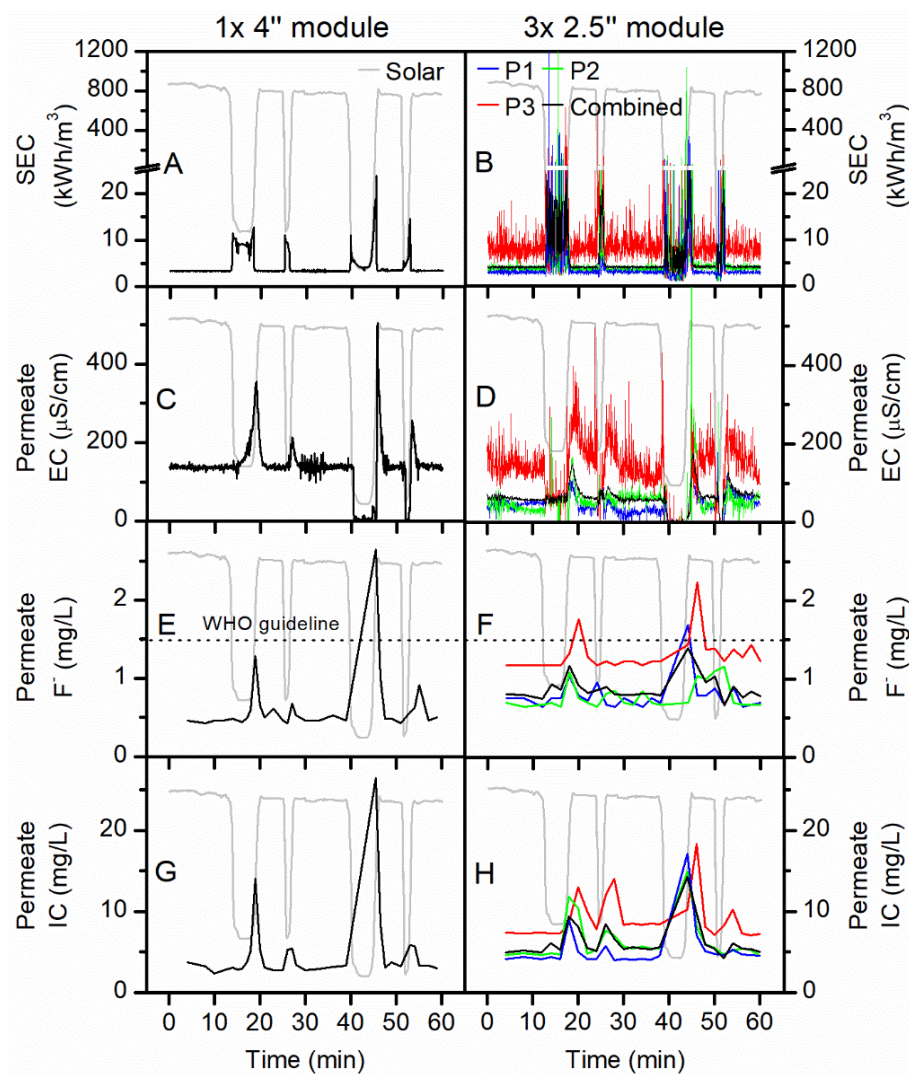
454 above, the higher rejecting BW30 was more sensitive to axial pressure drop than the NF270 because
455 of a higher osmotic pressure and thus a lower net driving pressure. Therefore the 3× 2.5" module
456 performed more poorly compared to the 1× 4" module when using BW30.
457



458
459 Figure 6 Comparison of the 1× 4" and 3× 2.5" modules of BW30 over 60 min of the solar day: (A,
460 B) pressure, (C, D) feed flow, (E, F) flux, (G, H) recovery.

461
462 It is noteworthy that the flux values of both modules dropped to 0 L/m².h during the light and
463 heavy cloud periods, which had a negative impact on the permeate quality. There was a spike in the
464 permeate EC upon the end of every cloud period. The zero permeate EC reading during the heavy
465 cloud period was because of air in the sensor (Figure 7C,D). The combined permeate EC of the 3×
466 2.5" module was lower than that of the 1× 4" module, due to the first and third elements of the 3×
467 2.5" module exhibiting remarkably efficient salt rejection (Figure 7D). In contrast, the third element
468 of the 3× 2.5" module performed rather poorly in this respect.

469 Regarding F^- and IC removal, the performance of $1 \times 4''$ module was better than the $3 \times 2.5''$
 470 module (Figure 7E–H). When analyzing individual elements of the $3 \times 2.5''$ module, the first two
 471 elements of the $3 \times 2.5''$ module exhibited good removal efficiency while the third element was
 472 inefficient in this regard. In fact, the performance of the third element was so poor that it was hardly
 473 worth having this element present in the module. It is noteworthy that the permeate F^- concentration
 474 of both modules temporarily exceeded the guideline value during the cloud periods. However, when
 475 considering that the permeate was continuously stored in a product tank, the system equipped with
 476 BW30 modules was able to produce safe drinking water in a long term, as will be discussed below.
 477



478
 479 Figure 7 Comparison of the $1 \times 4''$ and $3 \times 2.5''$ modules of BW30 over 60 min of the solar day: (A,
 480 B) SEC, (C, D) permeate EC, (E, F) permeate F^- concentration, (G, H) permeate IC concentration.
 481

482 3.5. Overall comparison of the 1×4" and 3×2.5" modules

483 As discussed above, the performance of the 1×4" and 3×2.5" modules of the NF270 and
484 BW30 membranes were evaluated and compared respectively during both cloudless and cloudy
485 periods. The overall performances of these modules were characterized by two parameters: the first
486 parameter is the cumulative sum of permeate water volume over time, which represents the
487 productivity of the module; the second parameter is the cumulative sum of permeate F⁻ concentration
488 over time, which indicates the permeate quality when continuously collected in a tank. The results
489 are shown in Figure 8, along with the results for two other 1×4" modules (NF90 and BW30LE) and
490 one 3×2.5" module (XLE), for which the complete performance data are presented in the
491 Supplementary Information. The flux for the first two 2.5" elements is higher than the flux for the
492 4" element, while permeate F⁻ concentration of the 2.5" elements is higher (2 mg/L) than that of the
493 4" inch element (<1 mg/L). This is somewhat anomalous and because the XLE membrane is not
494 usually included in this research no clear explanation for observation can be provided. Possibly this
495 performance is due to a quality variation between the individual elements.

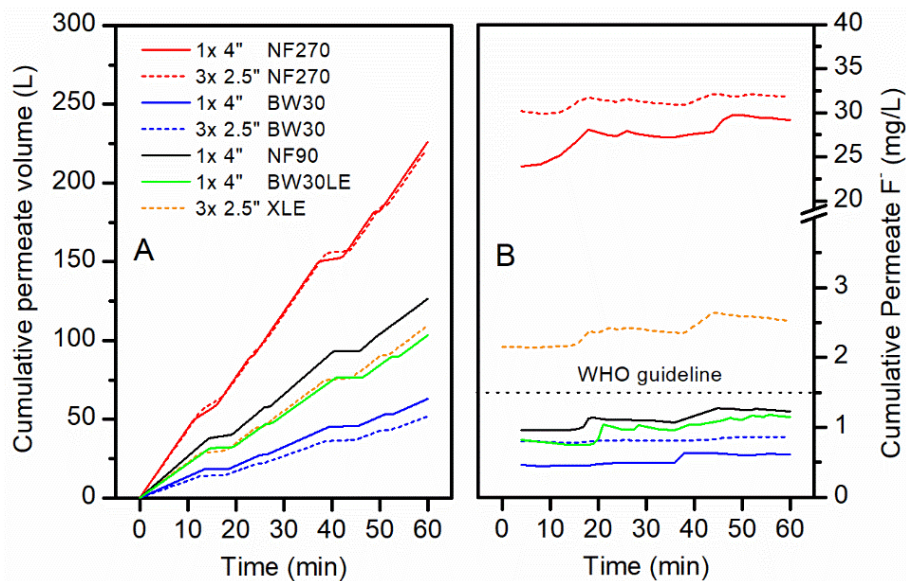
496 The cumulative permeate volume of all modules increased linearly with time, apart from
497 during the cloud periods when the productivity was reduced for a short time (Figure 8A). In case of
498 NF270, the permeate volumes produced by both modules were nearly the same (222 – 226 L),
499 whereas for BW30 the 1×4" module (63 L) produced a higher permeate volume than the 3×2.5"
500 module (52 L). The other three modules contained tight NF (NF90) and low energy RO (BW30LE,
501 XLE) membranes. Their water productivities were around halfway between that of the loose NF
502 (NF270) and the tight RO (BW30) membranes. The overall order was as follows: 1×4" NF270 > 3×
503 2.5" NF270 > 1×4" NF90 > 3×2.5" XLE > 1×4" BW30LE > 1×4" BW30 > 3×2.5" BW30, which
504 was completely consistent with the order of the permeance values, as reported in Table 2.

505 The cumulative permeate F⁻ concentration of all modules increased in a stepped manner due
506 to the dramatic soar of transient concentration during the cloud periods (Figure 8B). It is evident that
507 the 1×4" module had a better performance than the 3×2.5" module for both NF270 and BW30. As
508 discussed above, the third element of the 3×2.5" module reduced the overall performance of the
509 module significantly, which was due to the increasing feed concentration and the greater pressure
510 drop along the feed channel. The cumulative permeate F⁻ concentration of all modules followed the
511 order: 3×2.5" NF270 > 1×4" NF270 > 3×2.5" XLE > 1×4" NF90 > 1×4" BW30LE > 3×2.5"
512 BW30 > 1×4" BW30. The order of membrane type was in good agreement with the salt rejection
513 data provided by the manufacturer [63]. Even though the cloudy periods did not contribute
514 substantially to water quality in this study, when longer cloud periods are experienced and

515 consequently the transients are even longer this contribution may need to be controlled to not
516 compromise the overall water quality. Long term tests will be required to evaluate this and the control
517 algorithm and hardware may be expanded to include a permeate flush for such periods.

518 When referring to the WHO guideline limit for F^- concentration of 1.5 mg/L, three 1× 4"
519 modules (1× 4" BW30, 1× 4" BW30LE and 1× 4" NF90) and one 3× 2.5" module (3× 2.5" BW30)
520 were able to meet the guideline throughout the 60-min period. The other three modules (3× 2.5"
521 NF270, 1× 4" NF270, and 3× 2.5" XLE), on the contrary, failed to produce permeate with acceptable
522 F^- concentrations. It should be noted that XLE, as a RO membrane, was designed to have a higher
523 salt rejection than NF90 [63]. The inferior F^- removal of 3× 2.5" XLE compared to 1× 4" NF90
524 revealed the significant impact of module size on the actual system performance. The 1× 4" NF90
525 module seemed to be the best option in balancing permeate productivity and quality, which produced
526 127 L of drinking water with 1.2 mg/L F^- within the 60-min period.

527 When it comes to the cost factor, the market price of three 2.5" elements is much higher than
528 that of one 4" element, let alone the extra associated costs for three elements, such as extra tubing and
529 pressure vessels. It is thus more cost-effective to use the 1× 4" module rather than the 3× 2.5" module.
530



531
532 Figure 8 Comparison of cumulative (A) permeate volume and (B) permeate F^- concentration for
533 different 1× 4" and 3× 2.5" modules over 60 min of the solar day.
534

535 4. Conclusions

536 This study investigated the impact of membrane module size on the performance of a
537 batteryless PV-powered membrane system under fluctuating solar conditions. Several NF/RO

538 membranes in two module sizes ($1 \times 4''$ and $3 \times 2.5''$) of the same membrane area were used to treat a
539 naturally fluoridated brackish water in a remote village in northern Tanzania.

540 Under steady-state conditions, the $1 \times 4''$ and $3 \times 2.5''$ modules of NF270 achieved good flux
541 ($33 - 35 \text{ L/m}^2\cdot\text{h}$) and SEC (0.98 kWh/m^3), but as expected, the permeate quality ($25 - 30 \text{ mg/L F}^-$)
542 was too poor to meet the drinking water guideline for fluoride. Meanwhile the $1 \times 4''$ and $3 \times 2.5''$
543 modules of BW30 exhibited much lower flux ($8 - 12 \text{ L/m}^2\cdot\text{h}$) and correspondingly a higher SEC (3
544 $- 4 \text{ kWh/m}^3$), but the permeate F^- concentration ($0.5 - 0.8 \text{ mg/L}$) was satisfactory for drinking
545 purposes.

546 Under fluctuating solar conditions, the pressure and feed flow of the modules decreased
547 drastically, thus reducing the flux and increasing the SEC. The permeate water quality degraded
548 sharply because of the severe drop in flux. The transient permeate F^- concentration of BW30 modules
549 temporarily exceeded the guideline value. However, if being collected in a product tank, the
550 cumulative permeate F^- concentration of BW30 could always meet the WHO drinking water
551 guideline. The NF90 and BW30LE modules also achieved very good performance.

552 The performance of the $1 \times 4''$ module was always equivalent to or better than that of the $3 \times$
553 $2.5''$ module of the same membrane. This was mainly because the third element of the $3 \times 2.5''$ module
554 decreased the overall performance of the module substantially. Taking into account the cost factor,
555 large diameter SW modules enable considerable reductions in capital cost and life-cycle cost, thereby
556 increasing the economic feasibility of implementing PV-powered membrane systems in remote and
557 rural locations. Future work will focus on development of appropriate modelling frameworks for
558 performance simulation of PV-powered membrane systems during both steady-state and fluctuating
559 operations.

560

561 **5. Acknowledgements**

562 The research was funded in part by two Leverhulme Royal Society Africa Awards SADWAT-
563 Tanzania and SUCCESS; as well as the Helmholtz Association Recruitment Initiative for AIS and
564 BSR. The Energy Technology Partnership (ETP) and Drinking Water Quality Regulator for Scotland
565 (DWQR) provided the PhD scholarship for JS. The DOW Chemical Company kindly donated the
566 NF/RO membrane modules for this project, and GE Power & Water (Zenon) the UF module. Godfrey
567 Mkongo (Ngurdoto Defluoridation Research Station (NDRS), Tanzania) is greatly appreciated for his
568 hospitality when carrying out experiments at NDRS. William Dahi (Defluoridation Technology
569 Project, Tanzania) carried out the analysis of a huge number of samples, while Elly Karle and
570 Reinhard Sembritzki (KIT, Germany) provided IC and ICP data the source water sample. Minh

571 Nguyen (KIT, Germany) is thanked for drawing the graphic of the spiral wound element in the SI.
572 Prof Jack Gilron (BGU, Israel) has inspired this work through his questions at the PhD defense of
573 Gavin Park.
574

575 **6. Supplementary Information**

576 The SI contains a schematic of a spiral wound module, as well as further data of the NF90,
577 BW30LE and XLE membranes.

578 **7. References**

579 [1] J. Alcamo, N. Fernandez, S.A. Leonard, P. Peduzzi, A. Singh, R. Harding Rohr Reis, 21 issues
580 for the 21st Century: results of the UNEP Foresight Process on Emerging Environmental issues,
581 (2012).

582 [2] B.S. Richards, J. Shen, A.I. Schäfer, Water–energy nexus perspectives in the context of
583 photovoltaic-powered decentralized water treatment systems: A Tanzanian case study, *Energy*
584 *Technology*, (2017) 1-13.

585 [3] A.I. Schäfer, A. Broeckmann, B.S. Richards, *Renewable Energy Powered Membrane Technology*.
586 1. Development and Characterization of a Photovoltaic Hybrid Membrane System, *Environmental*
587 *Science & Technology*, 41 (2007) 998-1003.

588 [4] V.G. Gude, N. Nirmalakhandan, S. Deng, Renewable and sustainable approaches for desalination,
589 *Renewable and Sustainable Energy Reviews*, 14 (2010) 2641-2654.

590 [5] M. Shatat, M. Worall, S. Riffat, Opportunities for solar water desalination worldwide: Review,
591 *Sustainable Cities and Society*, 9 (2013) 67-80.

592 [6] D. Herold, A. Neskakis, A small PV-driven reverse osmosis desalination plant on the island of
593 Gran Canaria, *Desalination*, 137 (2001) 285-292.

594 [7] M. Thomson, D. Infield, A photovoltaic-powered seawater reverse-osmosis system without
595 batteries, *Desalination*, 153 (2003) 1-8.

596 [8] A. Chafidz, E.D. Kerme, I. Wazeer, Y. Khalid, A. Ajbar, S.M. Al-Zahrani, Design and fabrication
597 of a portable and hybrid solar-powered membrane distillation system, *Journal of Cleaner Production*,
598 133 (2016) 631-647.

599 [9] S.M. Shalaby, Reverse osmosis desalination powered by photovoltaic and solar Rankine cycle
600 power systems: A review, *Renewable and Sustainable Energy Reviews*, 73 (2017) 789-797.

601 [10] J. Shen, B.S. Richards, A.I. Schäfer, Renewable energy powered membrane technology: Case
602 study of St. Dorcas borehole in Tanzania demonstrating fluoride removal via nanofiltration/reverse
603 osmosis, *Separation and Purification Technology*, 170 (2016) 445-452.

604 [11] A. Joyce, D. Loureiro, C. Rodrigues, S. Castro, Small reverse osmosis units using PV systems
605 for water purification in rural places, *Desalination*, 137 (2001) 39-44.

- 606 [12] T. Espino, B. Peñate, G. Piernavieja, D. Herold, A. Neskakis, Optimised desalination of seawater
607 by a PV powered reverse osmosis plant for a decentralised coastal water supply, *Desalination*, 156
608 (2003) 349-350.
- 609 [13] M.A. Alghoul, P. Poovanaesvaran, M.H. Mohammed, A.M. Fadhil, A.F. Muftah, M.M. Alkilani,
610 K. Sopian, Design and experimental performance of brackish water reverse osmosis desalination unit
611 powered by 2 kW photovoltaic system, *Renewable Energy*, 93 (2016) 101-114.
- 612 [14] B.S. Richards, D.P.S. Capão, A.I. Schäfer, Renewable energy powered membrane technology.
613 2. The effect of energy fluctuations on performance of a photovoltaic hybrid membrane system,
614 *Environmental Science & Technology*, 42 (2008) 4563-4569.
- 615 [15] E.S. Mohamed, G. Papadakis, E. Mathioulakis, V. Belessiotis, A direct coupled photovoltaic
616 seawater reverse osmosis desalination system toward battery based systems — a technical and
617 economical experimental comparative study, *Desalination*, 221 (2008) 17-22.
- 618 [16] M. Thomson, D. Infield, Laboratory demonstration of a photovoltaic-powered seawater reverse-
619 osmosis system without batteries, *Desalination*, 183 (2005) 105-111.
- 620 [17] B.S. Richards, D.P.S. Capão, W.G. Früh, A.I. Schäfer, Renewable energy powered membrane
621 technology: Impact of solar irradiance fluctuations on performance of a brackish water reverse
622 osmosis system, *Separation and Purification Technology*, 156, Part 2 (2015) 379-390.
- 623 [18] L.A. Richards, B.S. Richards, A.I. Schäfer, Renewable energy powered membrane technology:
624 Salt and inorganic contaminant removal by nanofiltration/reverse osmosis, *Journal of Membrane
625 Science*, 369 (2011) 188-195.
- 626 [19] Dow Water and Process Solutions, FILMTEC™ Reverse Osmosis Membranes Technical
627 Manual,
628 http://msdssearch.dow.com/PublishedLiteratureDOWCOM/dh_095b/0901b8038095b91d.pdf?filepath=/609-00071.pdf&fromPage=GetDoc. Access date: May.
629
- 630 [20] J. Shen, G. Mkongo, G. Abbt-Braun, S.L. Ceppi, B.S. Richards, A.I. Schäfer, Renewable energy
631 powered membrane technology: Fluoride removal in a rural community in northern Tanzania,
632 *Separation and Purification Technology*, 149 (2015) 349-361.
- 633 [21] J. Schwinge, P.R. Neal, D.E. Wiley, D.F. Fletcher, A.G. Fane, Spiral wound modules and spacers:
634 Review and analysis, *Journal of Membrane Science*, 242 (2004) 129-153.
- 635 [22] A.J. Karabelas, M. Kostoglou, C.P. Koutsou, Modeling of spiral wound membrane desalination
636 modules and plants – review and research priorities, *Desalination*, 356 (2015) 165-186.
- 637 [23] J. Johnson, M. Busch, Engineering aspects of reverse osmosis module design, *Desalination and
638 Water Treatment*, 15 (2010) 236-248.
- 639 [24] A.J. Karabelas, C.P. Koutsou, M. Kostoglou, The effect of spiral wound membrane element
640 design characteristics on its performance in steady state desalination — A parametric study,
641 *Desalination*, 332 (2014) 76-90.
- 642 [25] J. Fawell, K. Bailey, J. Chilton, E. Dahi, L. Fewtrell, Y. Magara, Fluoride in drinking water,
643 World Health Organization, London 2006.

- 644 [26] J.P. Shorter, J. Massawe, N. Parry, R.W. Walker, Comparison of two village primary schools in
645 northern Tanzania affected by fluorosis, *International Health*, 2 (2010) 269-274.
- 646 [27] H.G. Jarvis, P. Heslop, J. Kisima, W.K. Gray, G. Ndossi, A. Maguire, R.W. Walker, Prevalence
647 and aetiology of juvenile skeletal fluorosis in the south-west of the Hai district, Tanzania – a
648 community-based prevalence and case-control study, *Tropical Medicine & International Health*, 18
649 (2013) 222-229.
- 650 [28] H. Mjengera, G. Mkongo, Appropriate defluoridation technology for use in flourotic areas in
651 Tanzania, *Physics and Chemistry of the Earth*, 28 (2003) 1097-1104.
- 652 [29] S. Ayoob, A.K. Gupta, V.T. Bhat, A conceptual overview on sustainable technologies for the
653 defluoridation of drinking water, *Critical Reviews in Environmental Science and Technology*, 38
654 (2008) 401-470.
- 655 [30] K.M.K. Kut, A. Sarswat, A. Srivastava, C.U. Pittman, D. Mohan, A review of fluoride in african
656 groundwater and local remediation methods, *Groundwater for Sustainable Development*, 2-3 (2016)
657 190-212.
- 658 [31] J. Shen, A.I. Schäfer, Factors affecting fluoride and natural organic matter (NOM) removal from
659 natural waters in Tanzania by nanofiltration/reverse osmosis, *Science of The Total Environment*,
660 527–528 (2015) 520-529.
- 661 [32] C. Onorato, M. Gaedtke, M. Kespe, H. Nirschl, A.I. Schäfer, Renewable energy powered
662 membrane technology: computational fluid dynamics evaluation of system performance with variable
663 module size and fluctuating energy, *Separation and Purification Technology*, (2019).
- 664 [33] World Health Organization, Guidelines for drinking-water quality: fourth edition incorporating
665 the first addendum, in, Geneva, 2017.
- 666 [34] A.I. Schäfer, A. Broeckmann, B.S. Richards, Renewable energy powered membrane technology.
667 1. development and characterization of a photovoltaic hybrid membrane system, *Environmental
668 Science & Technology*, 41 (2006) 998-1003.
- 669 [35] B.S. Richards, G.L. Park, T. Pietzsch, A.I. Schäfer, Renewable energy powered membrane
670 technology: Brackish water desalination system operated using real wind fluctuations and energy
671 buffering, *Journal of Membrane Science*, 468 (2014) 224-232.
- 672 [36] Dow Chemical Company, DOW FILMTEC Fibreglassed Elements for Light Industrial Systems,
673 <http://www.dupont.com/content/dam/Dupont2.0/Products/water/literature/609-00350.pdf>. Access
674 date: 12 November 2018.
- 675 [37] Dow Chemical Company, FILMTEC Membranes NF270 Nanofiltration Elements for
676 Commercial Systems,
677 <http://www.dupont.com/content/dam/Dupont2.0/Products/water/literature/609-00519.pdf>. Access
678 date: 12 November 2018.
- 679 [38] Dow Chemical Company, DOW FILMTEC Membranes DOW FILMTEC NF90 Nanofiltration
680 Elements for Commercial Systems,
681 <http://www.dupont.com/content/dam/Dupont2.0/Products/water/literature/609-00378.pdf>. Access
682 date: 12 November 2018.

- 683 [39] Dow Chemical Company, FILMTEC Membranes Basics of RO and NF: Element Characteristics,
684 http://msdssearch.dow.com/PublishedLiteratureDOWCOM/dh_0071/0901b803800710df.pdf.
685 Access date: 12 November 2018.
- 686 [40] Dow Chemical Company, FILMTEC Membranes System Design: Introduction,
687 http://msdssearch.dow.com/PublishedLiteratureDOWCOM/dh_0043/0901b803800435bd.pdf?filepa
688 [th=liquidseps/pdfs/noreg/609-02046.pdf](http://msdssearch.dow.com/PublishedLiteratureDOWCOM/dh_0043/0901b803800435bd.pdf?filepath=liquidseps/pdfs/noreg/609-02046.pdf). Access date: 12 November 2018.
- 689 [41] Dow Chemical Company, FILMTEC XLE-2540 Membranes - Extra Low Energy Elements for
690 Commercial Systems,
691 <http://www.dupont.com/content/dam/Dupont2.0/Products/water/literature/609-00349.pdf>. Access
692 date: 12 November 2018.
- 693 [42] Dow Chemical Company, FILMTEC LE-4040 Membranes - Fiberglassed Elements for Light
694 Industrial Systems, <https://www.lenntech.com/Data-sheets/Dow-Filmtec-LE-4040.pdf>. Access date:
695 12 November 2018.
- 696 [43] B.S. Richards, G.L. Park, T. Pietzsch, A.I. Schäfer, Renewable energy powered membrane
697 technology: Safe operating window of a brackish water desalination system, *Journal of Membrane*
698 *Science*, 468 (2014) 400-409.
- 699 [44] A.I. Schäfer, J. Shen, B.S. Richards, Renewable energy powered membrane technology:
700 Removal of natural organic matter and fluoride in Tanzanian communities, *npj Nature Clean Water*,
701 24 (2018) 1-10.
- 702 [45] A.F. Derradji, S. Taha, G. Dorange, Application of the resistances in series model in
703 ultrafiltration, *Desalination*, 184 (2005) 377-384.
- 704 [46] G. Schock, A. Miquel, Mass transfer and pressure loss in spiral wound modules, *Desalination*,
705 64 (1987) 339-352.
- 706 [47] J. Mulder, *Basic Principles of Membrane Technology*, Springer, Netherlands, 1996.
- 707 [48] I.E. Idelchik, *Handbook of Hydraulic Resistance*, Begell House Publishers, USA, 2007.
- 708 [49] MathWorks, Hydraulic resistance in pipe bend,
709 <https://www.mathworks.com/help/phymod/hydro/ref/pipebend.html>. Access date: 12 November
710 2018.
- 711 [50] K. Boussu, Y. Zhang, J. Cocquyt, P. Van der Meeren, A. Volodin, C. Van Haesendonck, J.A.
712 Martens, B. Van der Bruggen, Characterization of polymeric nanofiltration membranes for systematic
713 analysis of membrane performance, *Journal of Membrane Science*, 278 (2006) 418-427.
- 714 [51] I. Owusu-Agyeman, A. Jeihanipour, T. Luxbacher, A.I. Schäfer, Implications of humic acid,
715 inorganic carbon and speciation on fluoride retention mechanisms in nanofiltration and reverse
716 osmosis, *Journal of Membrane Science*, 528 (2017) 82-94.
- 717 [52] H. Choi, K. Zhang, D.D. Dionysiou, D.B. Oerther, G.A. Sorial, Influence of cross-flow velocity
718 on membrane performance during filtration of biological suspension, *Journal of Membrane Science*,
719 248 (2005) 189-199.

- 720 [53] J.S. Vrouwenvelder, C. Picioreanu, J.C. Kruithof, M.C.M. van Loosdrecht, Biofouling in spiral
721 wound membrane systems: Three-dimensional CFD model based evaluation of experimental data,
722 Journal of Membrane Science, 346 (2010) 71-85.
- 723 [54] J. Luo, Y. Wan, Effects of pH and salt on nanofiltration - A critical review, Journal of Membrane
724 Science, 438 (2013) 18-28.
- 725 [55] S.M.J. Zaidi, F. Fadhillah, Z. Khan, A.F. Ismail, Salt and water transport in reverse osmosis thin
726 film composite seawater desalination membranes, Desalination, 368 (2015) 202-213.
- 727 [56] Y. Marcus, Thermodynamics of solvation of ions. Part 5.-Gibbs free energy of hydration at
728 298.15 K, Journal of the Chemical Society, Faraday Transactions, 87 (1991) 2995-2999.
- 729 [57] L.A. Richards, B.S. Richards, B. Corry, A.I. Schäfer, Experimental energy barriers to anions
730 transporting through nanofiltration membranes, Environmental Science & Technology, 47 (2013)
731 1968-1976.
- 732 [58] Seametrics, Resolving flowmeter instability problems, in, USA, 2009.
- 733 [59] G.H. Keulegan, K.H. Beij, Pressure Losses for Fluid Flow in Curved Pipes, US Government
734 Printing Office, USA, 1937.
- 735 [60] H.M. Laborde, K.B. França, H. Neff, A.M.N. Lima, Optimization strategy for a small-scale
736 reverse osmosis water desalination system based on solar energy, Desalination, 133 (2001) 1-12.
- 737 [61] C. Charcosset, A review of membrane processes and renewable energies for desalination,
738 Desalination, 245 (2009) 214-231.
- 739 [62] G.J. Kirmeyer, Guidance Manual for Monitoring Distribution System Water Quality, American
740 Water Works Association, USA, 2002.
- 741 [63] Dow Chemical Company, Dow Water and Process Solutions - Levels of Separation of IX, RO,
742 NF, UF, https://dowwater.custhelp.com/app/answers/detail/a_id/477. Access date: 12 November
743 2018.
744
745

746 **SUPPLEMENTARY INFORMATION**

747
748 **Renewable energy powered membrane technology: experimental**
749 **investigation of system performance with variable module size and fluctuating**
750 **energy**

751
752 *Junjie Shen^{1,2,3}, Azam Jeihanipour⁴, Bryce S. Richards^{2,4}, Andrea I. Schäfer^{3,5*}*

753
754 *¹ Centre for Advanced Separations Engineering, University of Bath, Bath BA2 7AY,*
755 *United Kingdom*

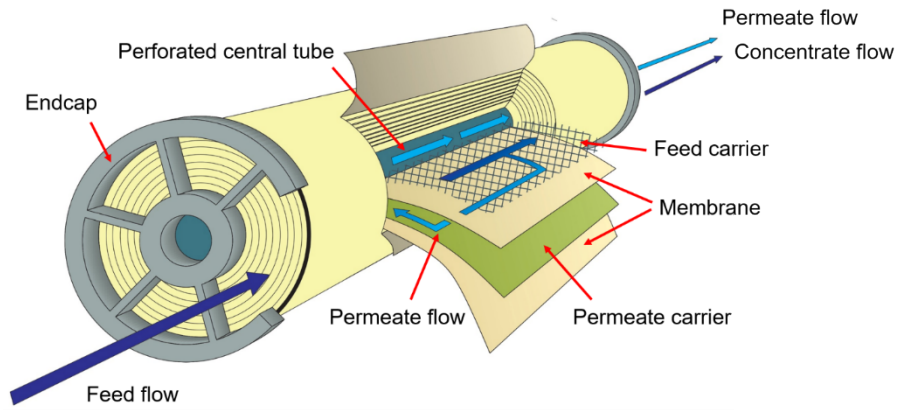
756 *² School of Engineering and Physical Sciences, Heriot-Watt University, Edinburgh*
757 *EH14 4AS, United Kingdom*

758 *³ Water and Environmental Science and Engineering, Nelson Mandela African Institute of*
759 *Science and Technology, Arusha, Tanzania*

760 *⁴ Institute of Microstructure Technology (IMT), KIT, Hermann-von-Helmholtz-Platz 1,*
761 *76344 Eggenstein-Leopoldshafen, Germany*

762 *⁵ Membrane Technology Department, Institute of Functional Interfaces (IFG-MT),*
763 *Karlsruhe Institute of Technology, Hermann-von-Helmholtz-Platz 1, 76344 Eggenstein-*
764 *Leopoldshafen, Germany*

779



780

781

782 Figure S1 Graphic of a spiral wound element

783

784

785

786

787

788

789

790

791

792

793

794

795

796

797

798

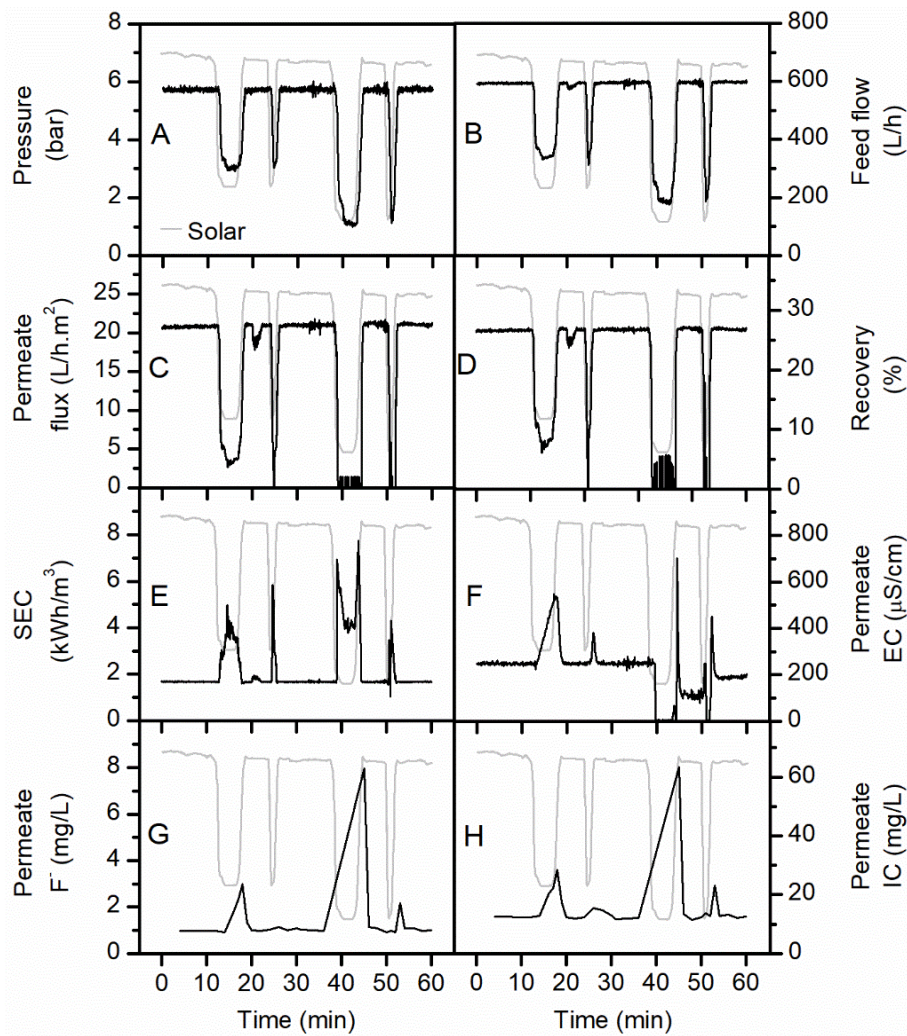
799

800

801

802

803



804

805

806

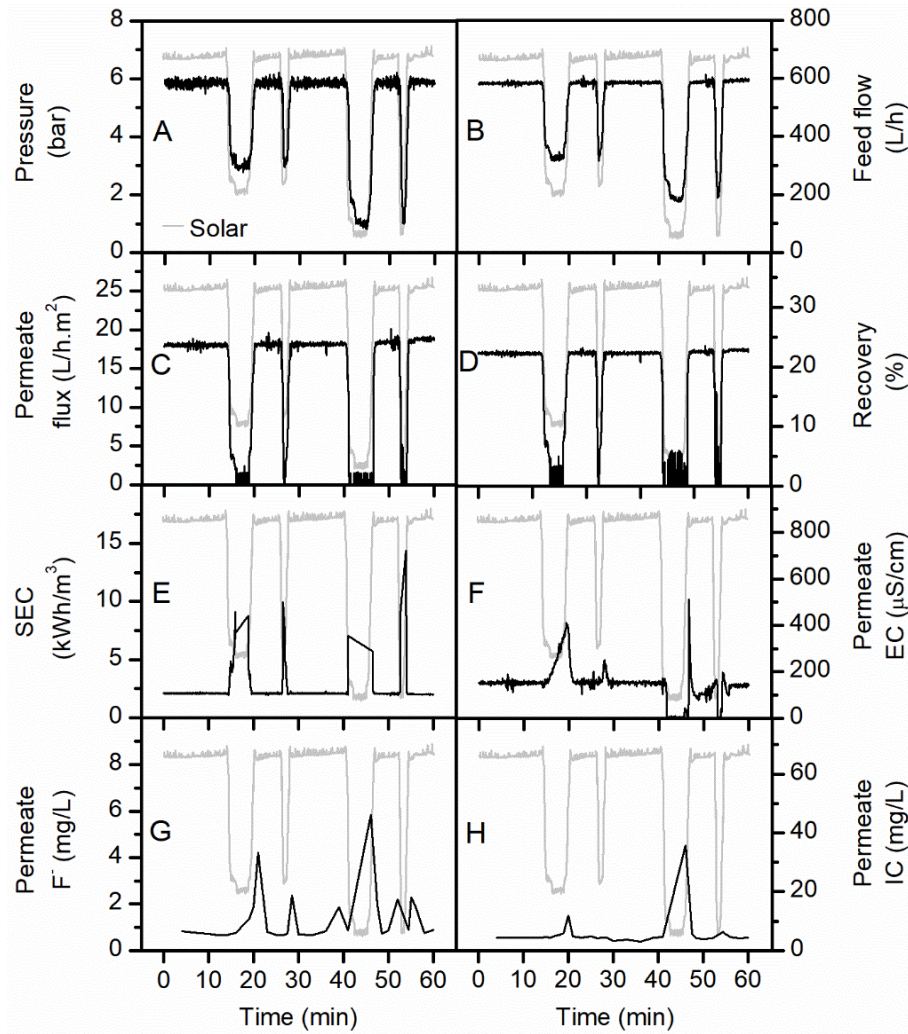
807

808

809

810

Figure S2 Instantaneous system performance of 1× 4" NF90 module over 60 min of the solar day: (A) pressure, (B) feed flow, (C) flux, (D) recovery, (E) SEC, (F) permeate EC, (G) permeate F⁻ concentration, (H) permeate IC concentration



812

813

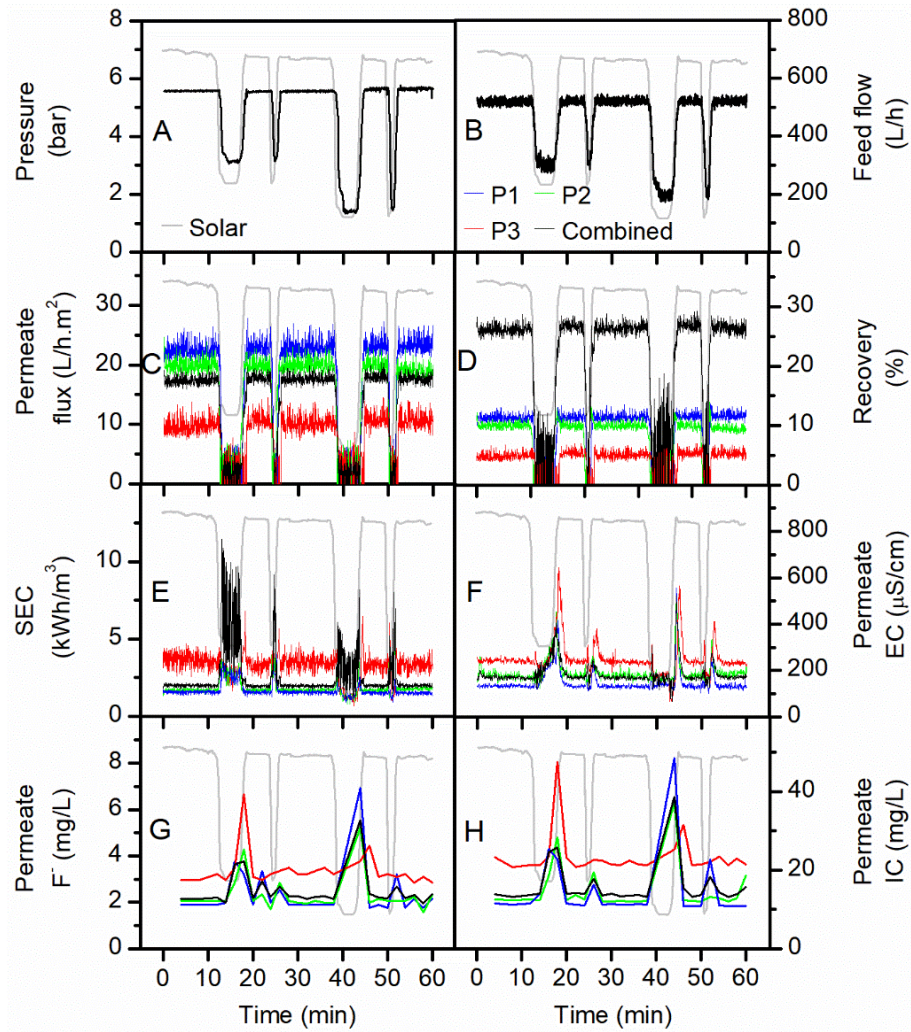
814

815

816

817

Figure S3 Instantaneous system performance of 1× 4" BW30LE module over 60 min of the solar day: (A) pressure, (B) feed flow, (C) flux, (D) recovery, (E) SEC, (F) permeate EC, (G) permeate F⁻ concentration, (H) permeate IC concentration



819

820

821

822

823

824

825

826

Figure S4 Instantaneous system performance of 3×2.5" XLE module over 60 min of the solar day: (A) pressure, (B) feed flow, (C) flux, (D) recovery, (E) SEC, (F) permeate EC, (G) permeate F⁻ concentration, (H) permeate IC concentration